Angewandte Chemie
Eine Zeitschrift der Gesellschaft Deutscher Chemiker

Supporting Information

A Dual-Color Fluorescent Probe Allows Simultaneous Imaging of Main and Papain-like Proteases of SARS-CoV-2-Infected Cells for Accurate Detection and Rapid Inhibitor Screening

Y. Cheng, R. M. Borum, A. E. Clark, Z. Jin, C. Moore, P. Fajtová, A. J. O'Donoghue, A. F. Carlin, J. V. Jokerst**

Author Contributions

J.J. Conceptualization:Lead; Data curation:Lead; Formal analysis:Lead; Funding acquisition:Lead; Project administration:Lead; Resources:Lead; Supervision:Lead; Validation:Lead; Visualization:Lead; Writing – original draft:Equal; Writing – review & editing:Lead
Y.C. Conceptualization:Lead; Data curation:Lead; Formal analysis:Lead; Investigation:Lead; Methodology:Lead; Validation:Lead; Visualization:Lead; Writing – original draft:Lead; Writing – review & editing:Lead
R.B. Data curation:Supporting; Formal analysis:Supporting; Visualization:Supporting; Writing – review & editing:Supporting
A.C. Methodology:Supporting; Validation:Supporting; Visualization:Supporting; Writing – review & editing:Supporting
Z.J. Data curation:Supporting; Formal analysis:Supporting; Investigation:Supporting; Methodology:Supporting; Visualization:Supporting; Writing – review & editing:Supporting
C.M. Data curation:Supporting; Formal analysis:Supporting; Resources:Supporting; Writing – review & editing:Supporting
P.F. Data curation:Supporting; Formal analysis:Supporting; Resources:Supporting; Writing – review & editing:Supporting
A.O. Resources:Supporting; Supervision:Supporting; Writing – review & editing:Supporting
A.C. Data curation:Supporting; Formal analysis:Supporting; Funding acquisition:Supporting; Project administration:-Supporting; Resources:Supporting; Supervision:Supporting; Writing – review & editing:Supporting

Table of Contents

References

Supplementary Videos

Supplementary Video S1

Description: SARS-CoV-2 noninfected TMPRSS2-Vero cells incubated with 3MBP5, Hoechst33258 and AlexaFluor 488 antibody of anti-SARS-CoV-2 nucleocapsid.

Supplementary Video S2

Description: SARS-CoV-2 infected TMPRSS2-Vero cells incubated with 3MBP5, Hoechst33258 and AlexaFluor 488 antibody of anti-SARS-CoV-2 nucleocapsid.

Supplementary Video S3

Description: SARS-CoV-2 infected TMPRSS2-Vero cells incubated with 3MBP5, Hoechst33258 and AlexaFluor 488 antibody of anti-SARS-CoV-2 M^{pro}.

1. Materials and methods.

Rink-amide resin (particle size 100 to 150 mesh; loading 0.67 mmol/g), Fmoc-protected L-amino acids, and O-Benzotriazole-N, N, N', N'-tetramethyl-uronium-hexafluorophosphate (HBTU) were purchased from AAPPTec, LLC. (Kentucky, USA). Cyanine3 carboxylic acid, Cyanine5 azide and Cyanine5 maleimide were purchased from Lumiprobe, Inc. (Maryland, USA). BHQ-2 carboxylic acid was purchased from Biosearch Technologies, LGC. (Novato, USA). The 1-amino-11-azido-3, 6, 9-trioxaundecane and Hoechst 33258 were purchased from Combi-Blocks, Inc. (San Diego, USA). Tris(hydroxymethyl)aminomethane (Tris-base), Tris(hydroxymethyl)aminomethane hydrochlorideand (Tris-HCl), sodium ascorbate, copper (I) iodide, N, N-diisopropylethylamine (DIPEA), thrombin, hemoglobin, albumin bovine serum and resazurin based in vitro toxicology assay kit were purchased from Sigma-Aldrich (Missouri, USA).

SARS-CoV-2 M^{pro} plasmid and an influenza virus protein (A/PR8/1834 NP, PR8 in short) plasmid were a kind gift from Nicholas S. Heaton.[1] M^{pro} inhibitor GC376 was purchased from Selleckchem, LLC. (Houston, USA). SARS-CoV-2 PL^{pro} with C-terminal His-tag (No. QHD43415, amino acid (a.a.) Arg745-Pro1061) were a kind gift from the Shaun K. Olsen.[2] PL^{pro} with N-terminal His-tag (YP_009725299.1, a.a. Glu1564-Val1880) and SARS-CoV-2 PL^{pro} plasmid (NC_045512.2 (4955-5905 nt)) were purchased from Sino Biologicial, Inc. (Pennsylvania, USA). PL^{pro} without Tag (YP_009725299.1, a.a. Glu1564-Lys1878) was purchased from Creative Biolabs, Inc. (New York, USA). PL^{pro} inhibitor GRL0617 was purchased from MedChemExpress, LLC. (New Jersey, USA). SARS-CoV-2 nsp3 (PL^{pro}) antibody was purchased from Gene Tex, Inc. (California, USA). SARS-CoV-2 nsp5 (M^{pro}) antibody was purchased from Cell Signaling Technology, Inc. (USA). HEK 293T cells were a kind gift from Dr. Liangfang Zhang. All other reagents were obtained from commercial sources and used without further purification. Deionized water (18.2 MΩ·cm) used in all experiments was purified with a Milli-Q Academic water purification system (Millipore Corp., Billerica, MA, USA).

The ^{1}H and ^{13}C NMR spectra were measured on a Bruker ARX 300 NMR spectrometer using chloroform-d ($CDCl_3$-d) or dimethyl sulfoxide-d6 (DMSO-d6) as solvent and tetramethylsilane (TMS) as internal reference. Splitting patterns are reported as s (single), d (doublet), t (triplet), and m (multiplet). Peptides were synthesized using an AAPPTec Eclipse system through standard solid phase Fmoc syntheses on Rink-amide resin. Electrospray ionization mass spectrometry (ESI-MS) data was acquired by using a Micromass Quattro Ultima mass spectrometer. High resolution mass spectra (HRMS) were recorded on a Bruker microTOF II mass spectrometer system. High performance liquid chromatography (HPLC) was performed by using a Shimadzu LC-40 HPLC system under the wavelength of 195 nm, 550 nm, and 650 nm. The sample was dissolved in water solution or acetonitrile, applied on a Zorbax 300 BS, C18 column (5 um, 9.4x250mm) from Agilent, and eluted at 1.5 mL/min with a 40 min gradient from 10% to 95% solvent B where solvent A is water (0.05% TFA solution) and solvent B is acetonitrile (0.05% TFA solution). All products were purified by HPLC to reach purity of 95%. UV-Vis absorption and fluorescence spectra were performed on a Synergy H1 microplate reader (BioTek). Confocal laser scanning microscopy images were obtained on a Zeiss LSM880 confocal laser scanning microscope (Zeiss).

2. FRET calculation methods.

The rate of Förster resonance energy transfer (k_{FRET}) from an excited donor (*e.g.*, Cy3*/Cy5*) to a ground state acceptor (*e.g.*, BHQ) separated by a distance (*e.g.*, peptide spacer), r, is given by

$$\mathrm{Cy3^{*}-BHQ-Cy5^{*}} \xrightarrow{k_{FRET}} \mathrm{Cy3-BHQ^{*}-Cy5};\ k_{FRET} = \frac{1}{\tau_D} \times \left(\frac{R_0}{r}\right)^6 \quad (1)$$

where τ_D is the decay time of the donor alone and R_0 is the Förster radius estimated by

$$R_0 = 9.78 \times 10^3 \times (k^2 Q_D n_s^{-4} I)^{\frac{1}{6}} \qquad (\text{in Å unit}) \tag{2}$$

Here, a value of k^2 = 2/3 was applied for randomly oriented dipoles; Q_D is the PL quantum yield of dye donor, and n_s is the refractive index of solvent. *I* is the spectral overlap integral expressed as

$$I = \int_0^\infty PL_{D-corr}(\lambda)\varepsilon_A(\lambda)\lambda^4 d\lambda \tag{3}$$

where $PL_{D\text{-}corr}(\lambda)$ is the normalized donor emission spectrum and $\varepsilon_A(\lambda)$ is the molar absorption spectrum of the acceptor. Next, the FRET efficiency, E_{FRET}, is defined as:

$$E_{FRET} = \frac{k_{FRET}}{k_{FRET} + \tau_D^{-1}} = \frac{R_0^6}{R_0^6 + r^6} \tag{4}$$

Experimentally, the FRET efficiency is estimated from fluorescence measurements using

$$E_{FRET} = 1 - \frac{PL_{DA}}{PL_D} \tag{5}$$

where PL_D and PL_{DA} designate the PL intensity of the donor alone and donor interacting with the acceptors, respectively. The calculated separation distance (*r*) represents the length of the peptide linker. Table. S1 summarizes all FRET parameters extracted from the Cy3−BHQ−Cy5 peptide conjugates.

3. Molecular design and imaging mechanism.

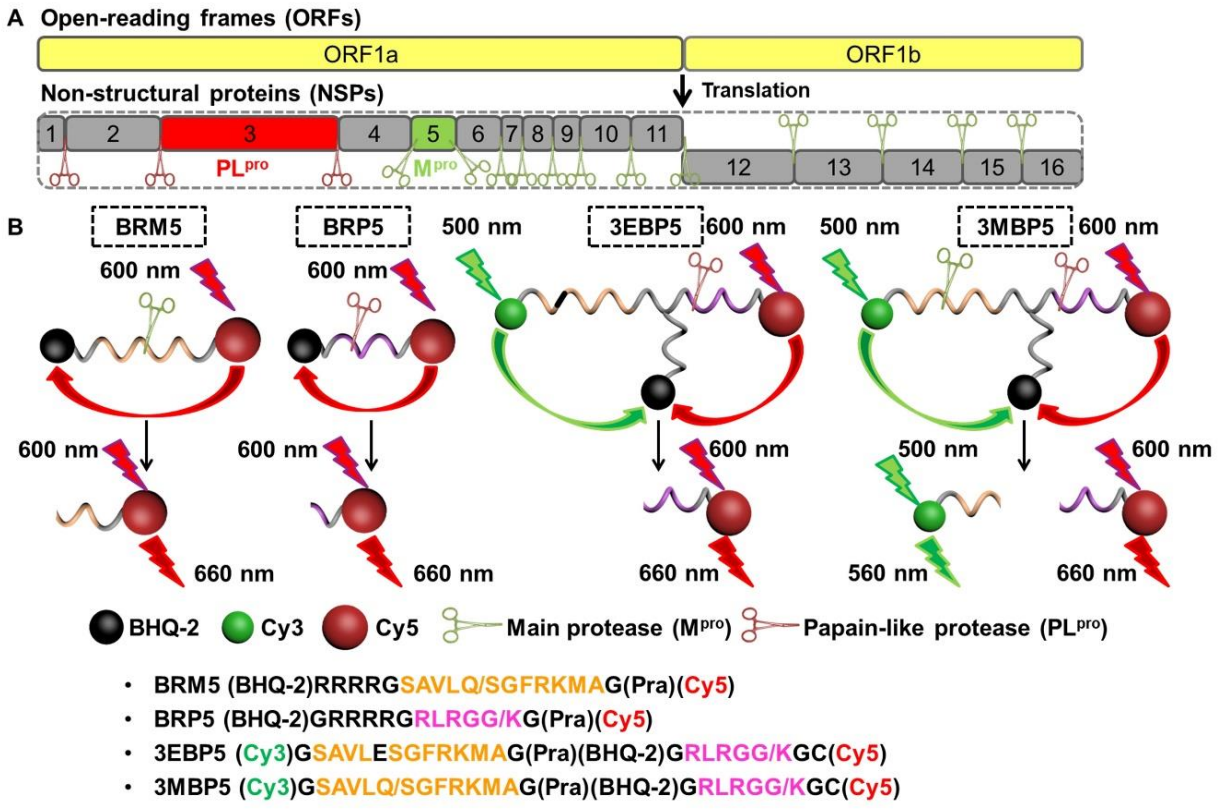

- BRM5 (BHQ-2)RRRRGSAVLQ/SGFRKMAG(Pra)(Cy5)
- BRP5 (BHQ-2)GRRRRGRLRGG/KG(Pra)(Cy5)
- 3EBP5 (Cy3)GSAVLESGFRKMAG(Pra)(BHQ-2)GRLRGG/KGC(Cy5)
- 3MBP5 (Cy3)GSAVLQ/SGFRKMAG(Pra)(BHQ-2)GRLRGG/KGC(Cy5)

Scheme S1. (A) Domain architecture of the SRAS-CoV-2 open-reading frames translated to non-structural proteins and cleavage sites of main protease (M^{pro}) and papain-like protease (PL^{pro}). (B) Mechanism and peptide sequences of BRM5, BRP5, 3EBP5 and 3MBP5 for M^{pro} and PL^{pro} detection.

SARS-CoV-2 M^{pro} sequence:[3]

SGFRKMAFPSGKVEGCMVQVTCGTTTLNGLWLDDVVYCPRHVICTSEDMLNPNYEDLLIRKSNHNFLVQAGNVQLRVIG
HSMQNCVLKLKVDTANPKTPKYKFVRIQPGQTFSVLACYNGSPSGVYQCAMRPNFTIKGSFLNGSCGSVGFNIDYDCVS
FCYMHHMELPTGVHAGTDLEGNFYGPFVDRQTAQAAGTDTTITVNVLAWLYAAVINGDRWFLNRFTTTLNDFNLVAMKY
NYEPLTQDHVDILGPLSAQTGIAVLDMCASLKELLQNGMNGRTILGSALLEDEFTPFDVVRQCSGVTFQ

SARS-CoV-2 PL^{pro} sequence (a.a. Arg1561-Gly1886):[3]

SL**RE**VRTIKVFTTVDNINLHTQVVDMSMTYGQQFGPTYLDGADVTKIKPHNSHEGKTFYVLPNDDTLRVEAFEYYHTTDP
SFLGRYMSALNHTKKWKYPQVNGLTSIKWADNNCYLATALLTLQQIELKFNPPALQDAYYRARAGEAANFCALILAYCNK
TVGELGDVRETMSYLFQHANLDSCKRVLNVVCKTCGQQQTTLKGVEAVMYMGTLSYEQFKKGVQIPCTCGKQATKYLV
QQESPFVMMSAPPAQYELKHGTFTCASEYTGNYQCGHYKHITSKETLYCIDGALLTKSSEYKGPITDVFYKENSYTTTI**KP
V**TYKLDG

4. Synthesis and Characterization

(1) Crude peptide synthesis: 100 mg Rink amide resin was chosen in solid-phase peptide synthesis. 2 x 4 mL 20% piperidine in DMF, 0.1 M amino acid in 3 mL DMF (5 equivalents), 0.1 M HBTU in 3 mL DMF (5 equivalents), and 0.2 M DIPEA in 3 mL DMF (10 equivalents) were used for each coupling cycle under the protection of nitrogen.

(2) Coupling with BHQ-2 or Cy3: After the completion of solid phase synthesis, 50 mg resin with crude peptide was transferred to a single-necked flask, and mixed with 0.1 M HBTU in 0.5 mL DMF and 0.2 M DIPEA in 0.5 mL DMF to further stir with BHQ-2 (5.0 mg, 7.2 μmol) or Cy3 carboxylic acid (5.0 mg, 10.1 μmol) reacting with the N-terminal amino group at room temperature (RT) for overnight. Resins with crude peptide BHQ-2 or Cy3 were added to a suitable filter and separately washed three times with DMF and CH_2Cl_2 to remove the unreacted reagents. Furthermore, peptides with BHQ-2 or Cy3 were cleaved off the resins by treating with cleavage cocktail containing 2.5 % thioanisole, 3% TIPS, 2.5% water, and 92% TFA for 3 hours followed by filtration to remove resin. Peptides were precipitated and centrifuged by addition of ice-cold diethyl ether to the filtrates. The residue was dissolved in 5 mL MeCN/H_2O (v/v=1:1) solution and lyophilized. Crude peptide with BHQ-2 or Cy3 was purified using semi-preparative HPLC.

(3) Coupling with Cy5:[4, 5] Cy5 maleimide (5.0 mg, 7.8 μmol) (or Cy5 azide (5.0 mg, 8.3 μmol), sodium ascorbate (0.8 mg, 4.2 μmol), copper (I) iodide (0.8 mg, 4.2 μmol)) and the purified peptides with BHQ-2 (4.2 μmol) or Cy3 (4.0 μmol) were dissolved in DMSO/H_2O (v/v=1:1) solution and stirred at 50 ^{0}C for 24 h under the protection of nitrogen. The crude peptide with BHQ-2 or Cy3 and Cy5 was purified using semi-preparative HPLC.

(4) Coupling with BHQ-2-N_3:[4, 6] BHQ-2-N_3 (5.0 mg, 7.1 μmol), sodium ascorbate (0.7 mg, 3.6 μmol), copper (I) iodide (0.7 mg, 3.6 μmol), and the purified peptide with Cy3 and Cy5 (3.6 μmol) were dissolved in DMSO/H2O (v/v=1:1) solution, and stirred at 50 ^{0}C for 24 h under protection of nitrogen. The crude peptide with BHQ-2, Cy3 and Cy5 was purified using semi-preparative HPLC.

4.1 Synthesis of BHQ-2-N_3.

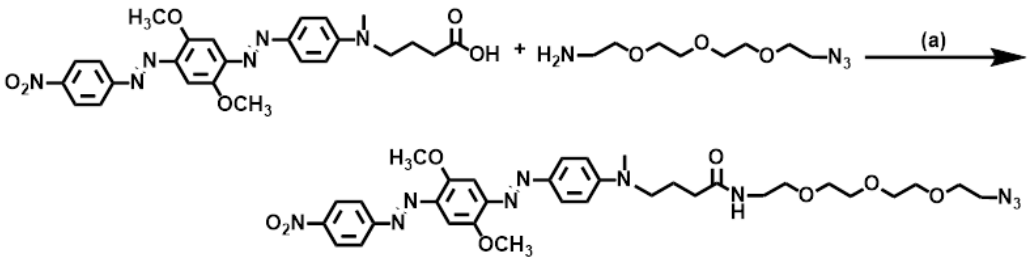

Scheme S2. The synthetic route of BHQ-2-N_3.

A solution of BHQ-2 (5.0 mg, 7.2 μmol), HBTU (8.3 mg, 22.0 μmol) and DIPEA (2.9 mg, 22.0 μmol) in DMF (1 mL) was stirred at RT for 30 min. Then, 1-amino-11-azido-3, 6, 9-trioxaundecane (2.4 mg, 11.0 μmol) was added and stirred at 50 ^{0}C for 24 h under the protection of nitrogen. RP-HPLC was used for purification and subsequent lyophilization yielded 4.5 mg the black powder product (yield 89%). The analytical HPLC estimated the purity of BHQ-2-N_3 at 96%. ^{1}H NMR (300 MHz, DMSO) δ 8.45 (d, J = 9.1 Hz, 2H), 8.07 (d, J = 9.1 Hz, 2H), 7.93 (t, J = 5.7 Hz, 1H), 7.83 (d, J = 9.2 Hz, 2H), 7.42 (d, J = 20.9 Hz, 2H), 6.89 (d, J = 9.4 Hz, 2H), 4.01 (s, 3H), 3.96 (s, 3H), 3.64 – 3.35 (m, 16H), 3.22 (q, J = 5.7 Hz, 2H), 3.07 (s, 3H), 2.17 (t, J = 7.1 Hz, 2H), 1.88 – 1.70 (m, 2H). HRMS (ESI) m/z: $[M+H]^{1+}$ calcd. for 707.3265; found, 707.4875. $[M+Na]^{1+}$ calcd. for 729.3085; found, 729.4531.

4.2 Synthesis of 3MBP5.

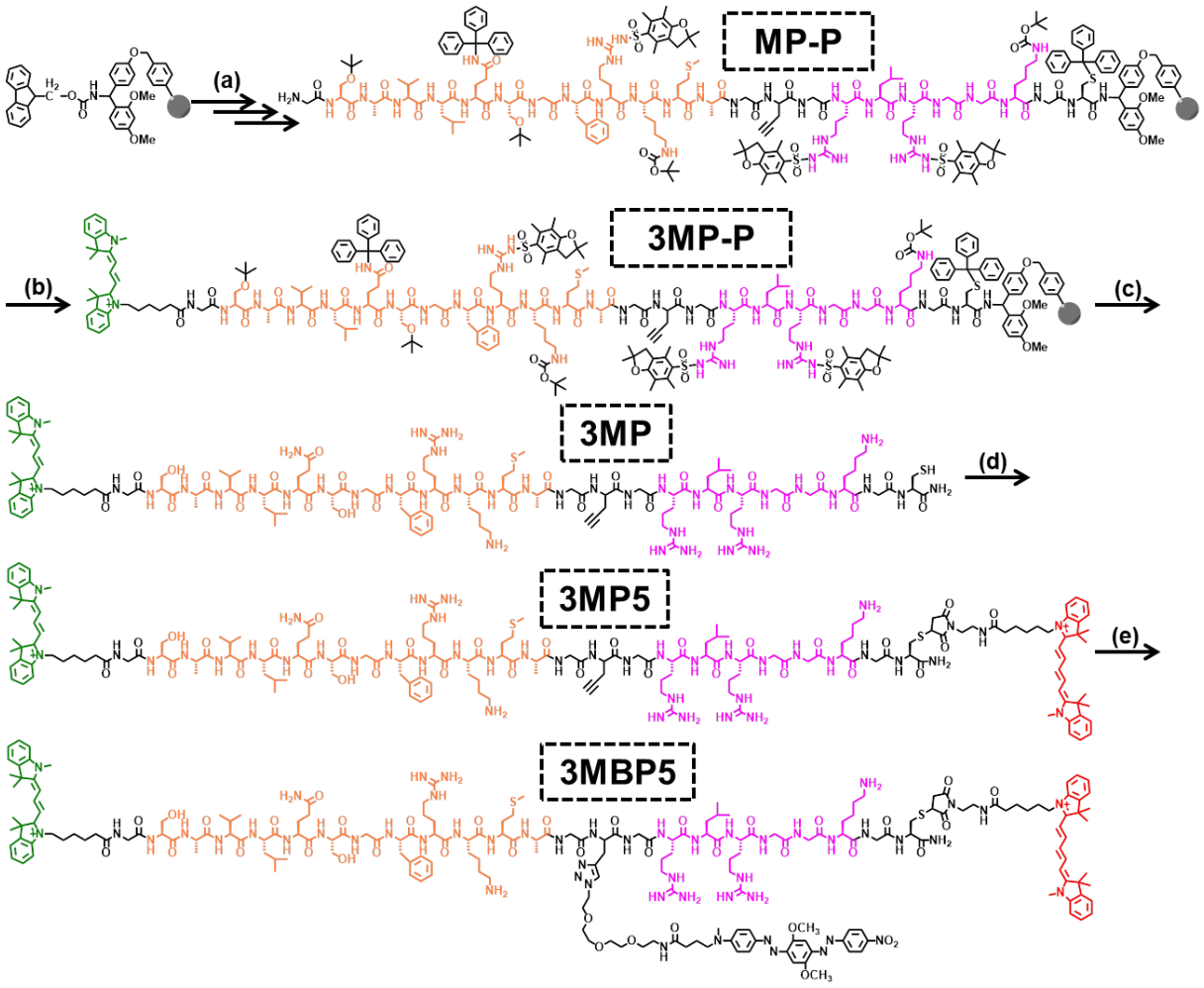

Scheme S3. The synthetic route of 3MBP5.

The main synthetic route of 3MBP5 is five steps through standard solid phase Fmoc synthesis, thiol−maleimide Michael addition and copper-catalyzed azide-alkyne click reaction. (a) Synthesis of MP-P. (b) Synthesis of 3MP-P. (c) Synthesis of 3MP, (17.5 mg, 56% yield based on the reactant of 5.0 mg Cy3). HRMS (ESI) m/z: $[M+3H]^{3+}/3$ calcd. for 942.8522; found, 943.6624. $[M+4H]^{4+}/4$ calcd. for 707.3911; found, 708.0201. $[M+5H]^{5+}/5$ calcd. for 566.1144; found, 566.6481. (d) Synthesis of 3MP5, (17.6 mg, 61% yield based on the reactant of 5.0 mg Cy5-MHS). HRMS (ESI) m/z: $[M+4H]^{4+}/4$ calcd. for 858.7283; found, 858.7753. $[M+5H]^{5+}/5$ calcd. for 687.1842; found, 687.3684. $[M+6H]^{6+}/6$ calcd. for 572.8214; found, 573.0051. $[M+7H]^{7+}/7$ calcd. for 491.1338; found, 491.2594. (e) Synthesis of 3MBP5, (7.8 mg, 45% yield based on the reactant of 14.5 mg 3MP5). HRMS (ESI) m/z: $[M+5H]^{5+}/5$ calcd. for 832.0489; found, 832.2641. $[M+6H]^{6+}/6$ calcd. for 693.5421; found, 693.7515. $[M+7H]^{7+}/7$ calcd. for 594.6086; found, 594.7490. The overall yield of 3MBP5 is 15.3%

4.3 Synthesis of 3EBP5.

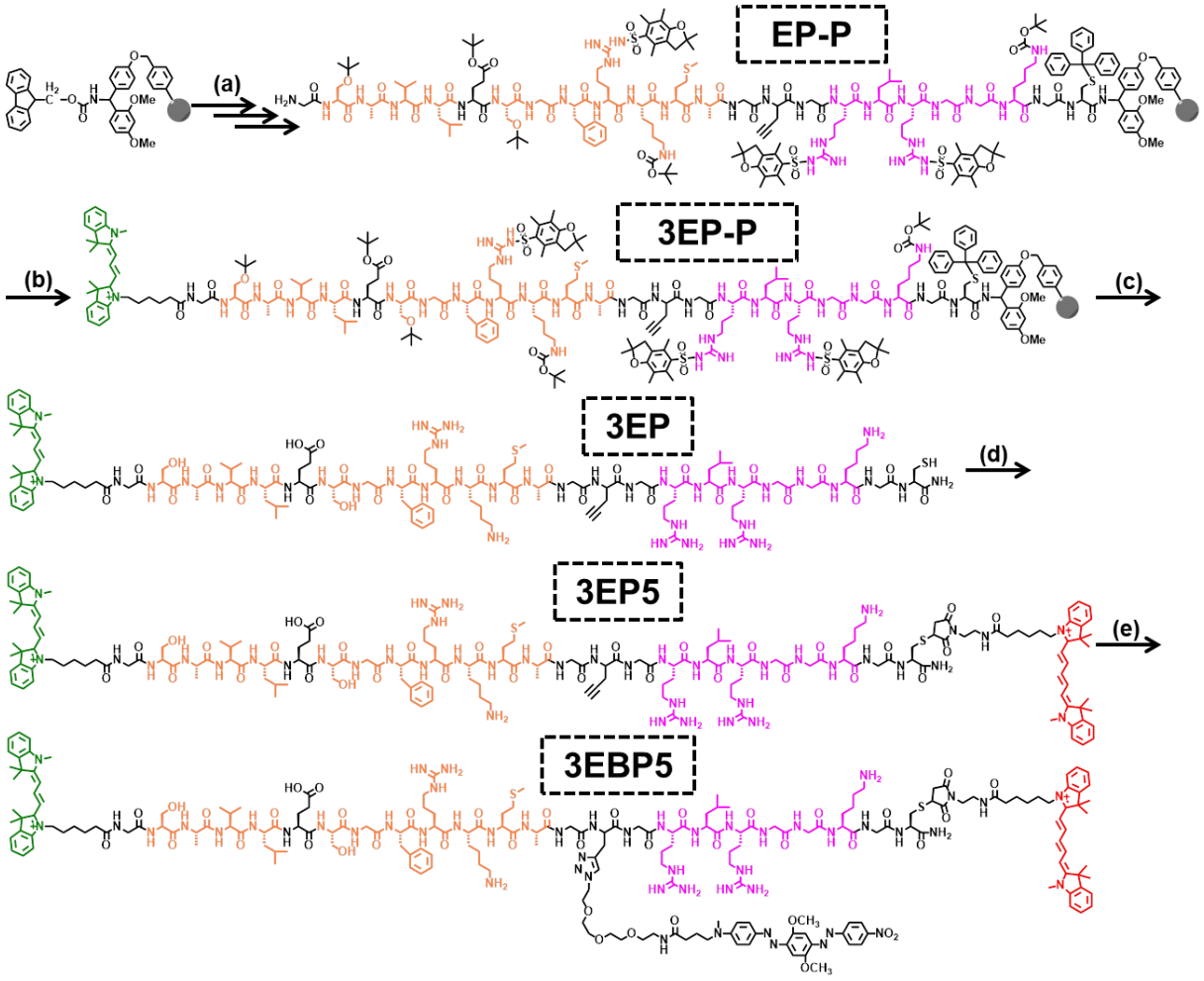

Scheme S4. The synthetic route of 3EBP5.

The main synthetic route of 3EBP5 is five steps through standard solid phase Fmoc synthesis, thiol-maleimide Michael addition and copper-catalyzed azide-alkyne click reaction. (a) Synthesis of EP-P. (b) Synthesis of 3EP-P. (c) Synthesis of 3EP, (10.9 mg, 59% yield based on the reactant of 3.0 mg Cy3). HRMS (ESI) m/z: $[M+3H]^{3+}/3$ calcd. for 943.1802; found, 943.4365. $[M+4H]^{4+}/4$ calcd. for 707.6371; found, 708.0198. $[M+5H]^{5+}/5$ calcd. for 566.3112; found, 566.6880. $[M+6H]^{6+}/6$ calcd. for 472.0940; found, 472.4508. (d) Synthesis of 3EP5, (12.3 mg, 67% yield based on the reactant of 3.0 mg Cy5-MHS). HRMS (ESI) m/z: $[M+4H]^{4+}/4$ calcd. for 863.4757; found, 863.5660. $[M+5H]^{5+}/5$ calcd. for 690.9821; found, 691.1514. $[M+6H]^{6+}/6$ calcd. for 575.9864; found, 576.2270. $[M+7H]^{7+}/7$ calcd. for 493.8466; found, 493.8358. (e) Synthesis of 3EBP5, (4.3 mg, 34% yield based on the reactant of 10.0 mg 3EP5). HRMS (ESI) m/z: $[M+5H]^{5+}/5$ calcd. for 832.2457; found, 832.6839. $[M+6H]^{6+}/6$ calcd. for 693.7061; found, 693.8868. $[M+7H]^{7+}/7$ calcd. for 594.7492; found, 595.0661. The overall yield of 3EBP5 is 13.4%

4.4 Synthesis of BRM5.

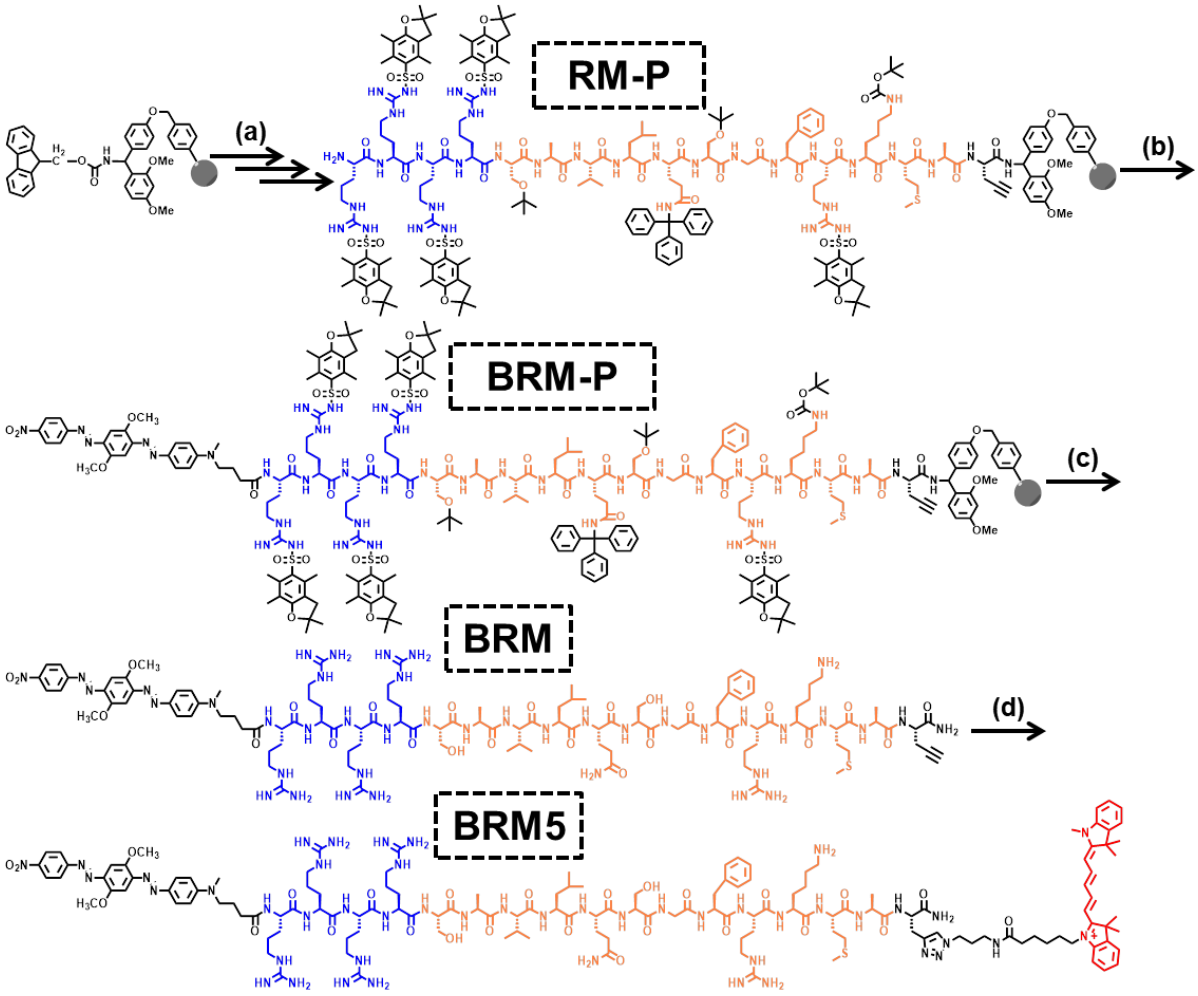

Scheme S5. The synthetic route of BRM5.

The main synthetic route of BRM5 is four steps through standard solid phase Fmoc synthesis and copper-catalyzed azide-alkyne click reaction: (a) Synthesis of RM-P. (b) Synthesis of BRM-P, (c) Synthesis of BRM, (4.3 mg, 39% yield based on the reactant of 3.0 mg BHQ-2). HRMS (ESI) m/z: $[M+3H]^{3+}$/3 calcd. for 834.4494; found, 835.04. $[M+4H]^{4+}$/4 calcd. for 626.0890; found, 626.62. $[M+5H]^{5+}$/5 calcd. for 501.0728; found, 501.55. (d) Synthesis of BRM5, (5.6 mg, 44% yield based on the reactant of 3.0 mg Cy5-N_3). HRMS (ESI) m/z: $[M+4H]^{4+}$/4 calcd. for 767.4302; found, 768.1829. $[M+5H]^{5+}$/5 calcd. for 614.1458; found, 614.4275. $[M+6H]^{6+}$/6 calcd. for 511.9561; found, 512.2394. The overall yield of BRM5 is 17.2%

4.5 Synthesis of BRP5.

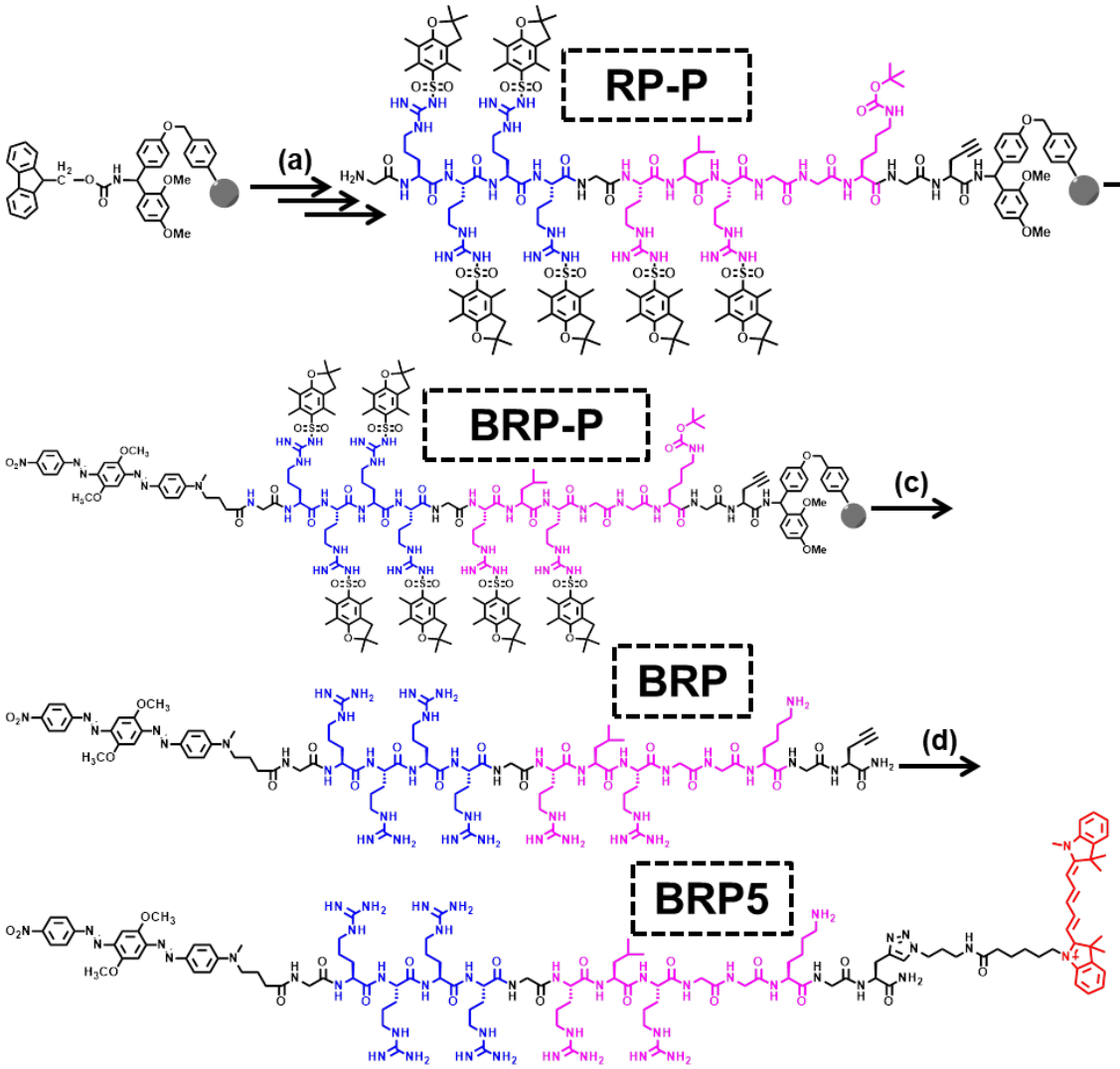

Scheme S6. The synthetic route of BRP5.

The main synthetic route of BRP5 is four steps through standard solid phase Fmoc synthesis and copper-catalyzed azide-alkyne click reaction. (a) Synthesis of RP-P, (b) Synthesis of BRP-P, (c) Synthesis of BRP, (4.5 mg, 40% yield based on the reactant of 3.0 mg BHQ-2). HRMS (ESI) m/z: $[M+3H]^{3+}/3$ calcd. for 688.7194; found, 689.1943. $[M+4H]^{4+}/4$ calcd. for 516.7915; found, 517.1635. $[M+5H]^{5+}/5$ calcd. for 413.6347; found, 413.9597. (d) Synthesis of BRP5, (5.2 mg, 41% yield based on the reactant of 3.0 mg Cy5-N_3). HRMS (ESI) m/z: $[M+4H]^{4+}/4$ calcd. for 658.1326; found, 658.4020. $[M+5H]^{5+}/5$ calcd. for 526.7076; found, 526.9604. $[M+6H]^{6+}/6$ calcd. for 439.0910; found, 439.2848. The overall yield of BRP5 is 16.4%

5. Enzymatic assay with BRM5, BRP5, 3EBP5, and 3MBP5.

The stock solution of BRM5, BRP5, 3EBP5, and 3MBP5 in 20 mM Tris buffer (pH=8.0) was diluted with M^{pro} and PL^{pro} assay buffer (20 mM Tris-HCl buffer (pH 8.0) with 150 mM NaCl, 1 mM DTT, and 5 % glycerol) to make a 2 μM working solution. Recombinant M^{pro} and PL^{pro} were added into the working solution and then diluted to a total of 100 μl or 200 μl with deionized water. The reaction mixture was incubated at 37 °C for 1 h for UV-Vis absorption and photoluminescence (PL) measurement. The solution was excited at 500 nm and 600 nm, and the emission was collected from 520 nm to 750 nm and 620 nm to 800 nm.

6. Cell culture and plasmid transfection.

HEK 293T cells were cultured in Dulbecco's Modified Eagle Medium (DMEM) with 10% fetal calf serum (FBS) and 1% penicillin streptomycin (PS, 10000 IU penicillin and 1000 μg/mL streptomycin, Multicell) in a cell culture plates at 37 °C in a humidified atmosphere containing 5% CO_2. For plasmid transfection, cells were treated with 100 μl to 1000 mL poly-L-lysine for 20 min before being seeded with HEK 293T cells. After 24 h incubation, Opti-MEM, plasmids (1 μg/μl to 3 μg/μl) and TransIT-LT (Mirus) were successively mixed and incubated at room temperature for 15 min before being added to cells dropwise according to the manufacturer’s instructions.

7. Incubation living cells with probes.

For confocal laser scanning microscopy imaging, HEK 293T cells or the plasmid transfected HEK 293T cells were seeded into cell culture dishes at a density of 2.0 × 105 in growth medium (DMEM supplemented with 10% FBS, 200 mL). After overnight incubation, the cells were washed with phosphate-buffered saline (PBS, pH 7.4) three times. A solution of the indicated probe in medium or PBS was then added, and the cells were incubated in a 5% CO_2 atmosphere at 37 °C for further use. Hoechst 33258 was subsequently added after the incubation of the probes. The supernatant was then discarded, and the cells were washed gently twice with PBS and fixed with 2% paraformaldehyde (PFA) at room temperature for 20 min prior to optical imaging.

8. Viral infection.

SARS-CoV-2 isolate WA1 (USA-WA1/2020, BEI NR-52281) was passaged once through primary human bronchial epithelial cells differentiated at air-liquid interface to select against furin site mutations. Virus was then expanded by one passage through TMPRSS2-Vero cells. Supernatants were clarified and stored at -80 °C, and titers were determined by fluorescent assay on TMPRSS2-Vero cells. TMPRSS2-Vero cells were infected with a multiplicity of infection (MOI) of 0.02 FFU per cell 24 h before incubation with probes. The SARS-CoV-2 noninfected and infected TMPRSS2-Vero cells were washed with Dulbecco's phosphate-buffered saline (DPBS) to remove FBS-containing media, then incubated with 2.0 μM 3MBP5 for 30 min and fixed with 4% formaldehyde. Cells were then stained using the nucleocapsid antibody or SARS-CoV-2 M^{pro} antibody and 5.0 μM Hoechst 33258. All work with SARS-CoV-2 was conducted in Biosafety Level-3 conditions at the University of California San Diego.

9. Immunofluorescence.

Fixed cells were washed with PBS, then with PBS including 1% BSA and 0.1% TritonX-100. Cells were incubated with primary antibody against SARS-CoV-2 nucleocapsid protein (1:2000, GeneTex, GTX135357) or M^{pro} (1:100, Cell Signaling Technology #51661) in PBS including 1% BSA and 0.1% TritonX-100 overnight at 4 °C. Cells were washed and incubated with AlexaFluor 488 goat anti-rabbit secondary antibody (Thermo Fisher Scientific) in PBS including 1% BSA for 1 h at room temperature, followed by 3x PBS washes.

10. Confocal laser scanning microscopy.

The fluorescence signals of cells were detected by using a Zeiss LSM880 confocal laser scanning microscope (Zeiss), equipped with a 63/1.42 numerical aperture oil-immersion objective lens. A 405 nm laser was chosen for the excitation of Hoechst 33258, the emission was collected at 420–460 nm. A 514 nm laser was chosen for the excitation of Cy3 and the emission was collected at 550–620 nm. A 633 nm laser was chosen for the excitation of Cy5 and the emission was collected at 650–735 nm. All fluorescence images were analyzed with Zeiss Image software (Zeiss).

11. Cytotoxicity assay.

The cytotoxic potential of Cy3, Cy5, 3MBP5, M^{pro}, PL^{pro}, GC376, and GRL0617 were assessed using the HEK 293T cells were respectively treated with Cy3 (2 μM, 10 μM and 20 μM), Cy5 (2 μM, 10 μM and 20 μM), 3MBP5 (2 μM, 10 μM and 20 μM), GC376 (1 μM, 5 μM and 10 μM), GRL0617 (1 μM, 5 μM and 10 μM), M^{pro} (0.2 μM, 1 μM and 2 μM) and PL^{pro} (0.2 μM, 1 μM and 2 μM), for 48 h in quadruplicate in a 96-well plate. The fluorescence of Resazurin solution at 690 nm using an excitation wavelength of 560 nm was recorded by a Synergy H1 microplate reader (BioTek) with standard operation procedures.

12. Western blotting analysis.

TMPRSS2-Vero cells were infected as above. At 24 h post-infection, cells were washed with PBS and lysed in RIPA buffer plus SDS added to 0.5% and supplemented with a protease inhibitor cocktail according to the protocol by the manufacturer. Total proteins were extracted and separated by sodium dodecyl sulfate-polyacrylamide gel electrophoresis (SDS-PAGE). The proteins were transferred to PVDF membranes. The membrane was blocked in 5% non-fat milk in TBS-T and probed with primary antibodies. Primary antibodies include anti-PL^{pro} (1:1000, GeneTex GTX135614), anti-M^{pro} (1:1000, Cell Signaling Technology #51661), anti-nucleocapsid (1:5000, Genetex GTX 135357), and anti-GAPDH (1:2000, Cell Signaling Technology). After washing with TBST, membranes were incubated with corresponding HRP-conjugated secondary antibody for 1 h at room temperature. The membrane was washed 3 times by TBST, developed with an enhanced chemiluminescent (ECL) kit, and imaged on a ChemiDoc MP.

Table. S1 Fluorophore photophysical properties, theoretical Förster radii (R_{DA}) and experimental Förster radii (r_{DA}) center-to-center separation distance between dye donor and dye acceptor in 3MP5 and 3MBP5.

	Theoretical calculation				**Experimental result**		
Fluorophore (D-A)	Ex.Coeff ($M^{-1}cm^{-1}$) (A)	Em/abs max (nm) (D/A)	Spectral overlap ($M^{-1}cm^{3}$)	R_{DA} (nm)	Laser (nm)	E_{FERT} (%)	r_{DA} (nm)
Cy3-Cy5	250000	560/640	$1.26x10^{-12}$	6.20	500	88.67	4.40
Cy3-BHQ-2	38000	560/560	$3.85x10^{-13}$	5.09	500	97.60	2.73
Cy5-BHQ-2	38000	660/560	$3.05x10^{-13}$	4.75	600	57.85	3.48.

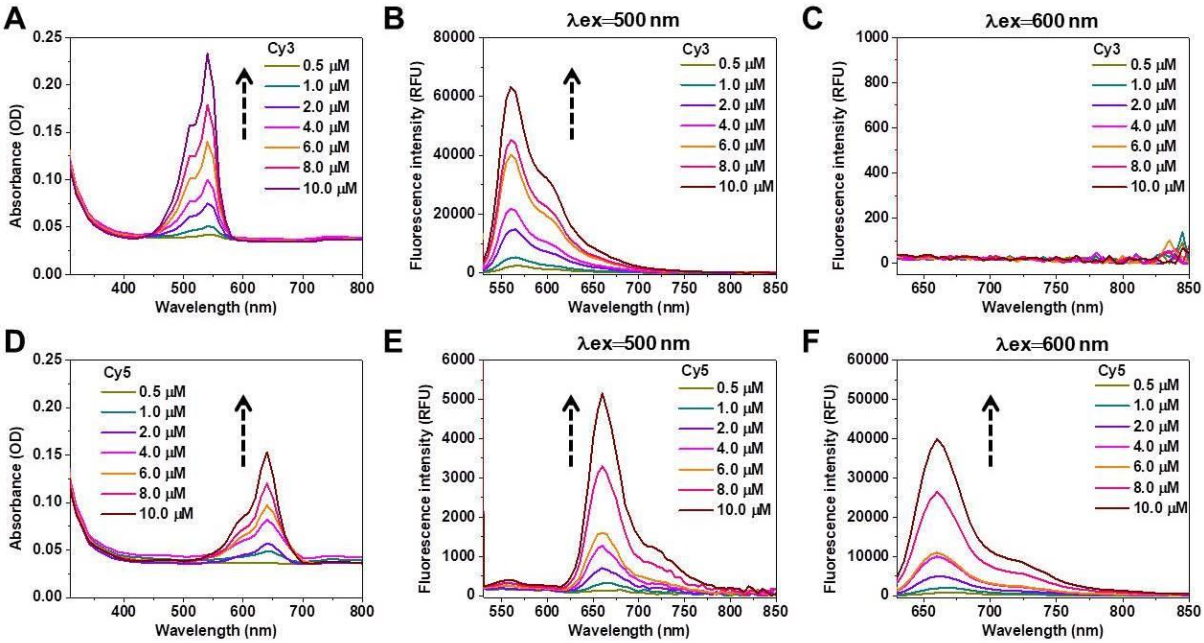

Figure S1. (A-C) UV−vis absorption and fluorescence spectra of (0.5 μM, 1.0 μM, 2.0 μM, 4.0 μM, 6.0 μM, 8.0 μM, and 10.0 μM) Cy3 in Tris-HCl buffer with 1% (v/v) DMSO. (D-F) UV−vis absorption and fluorescence spectra of (0.5 μM, 1.0 μM, 2.0 μM, 4.0 μM, 6.0 μM, 8.0 μM, and 10.0 μM) Cy5 in Tris-HCl buffer with 1% (v/v) DMSO. It shows that 500 nm for Cy3 and 600 nm for Cy5 were optimal excitation wavelengths to avoid overlap of emission spectra.

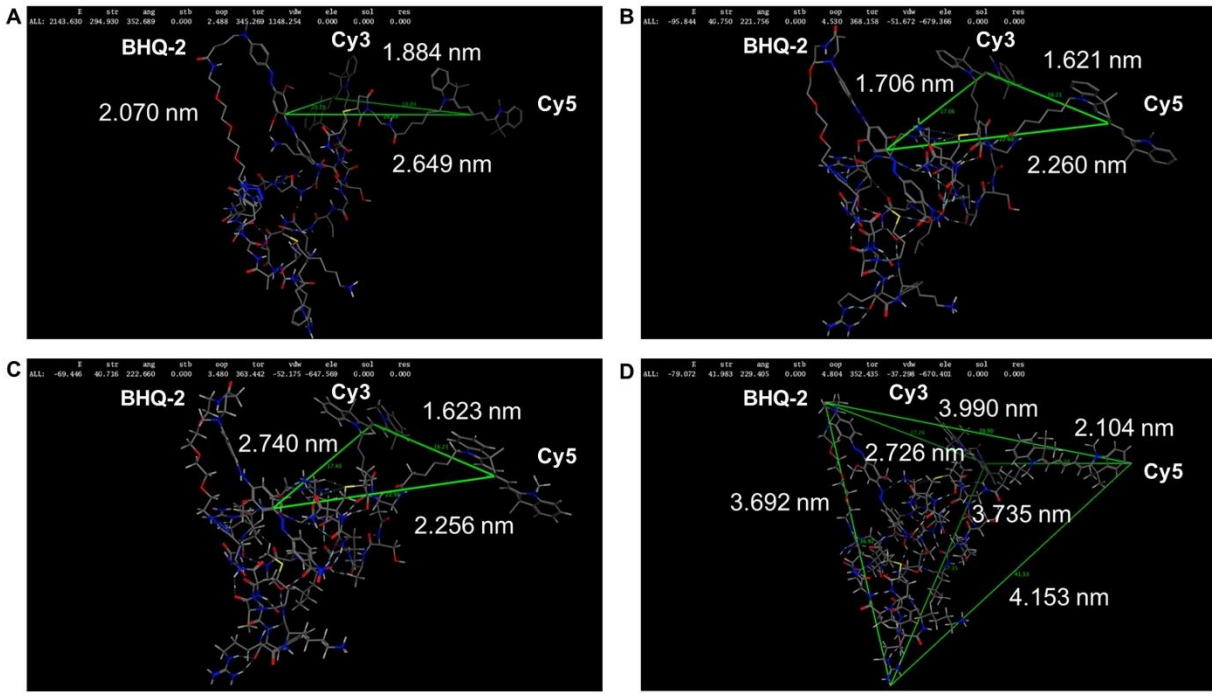

Figure S2. (A-C) The lowest energy structures and center-to-center separation distance between the fluorophores of 3MBP5 was calculated by the MM2 with ChemBio3D Ultra, quick prep with the Molecular Operating Environment (MOE), and minimized MOE. (D). Molecular dimension of 3MBP5.

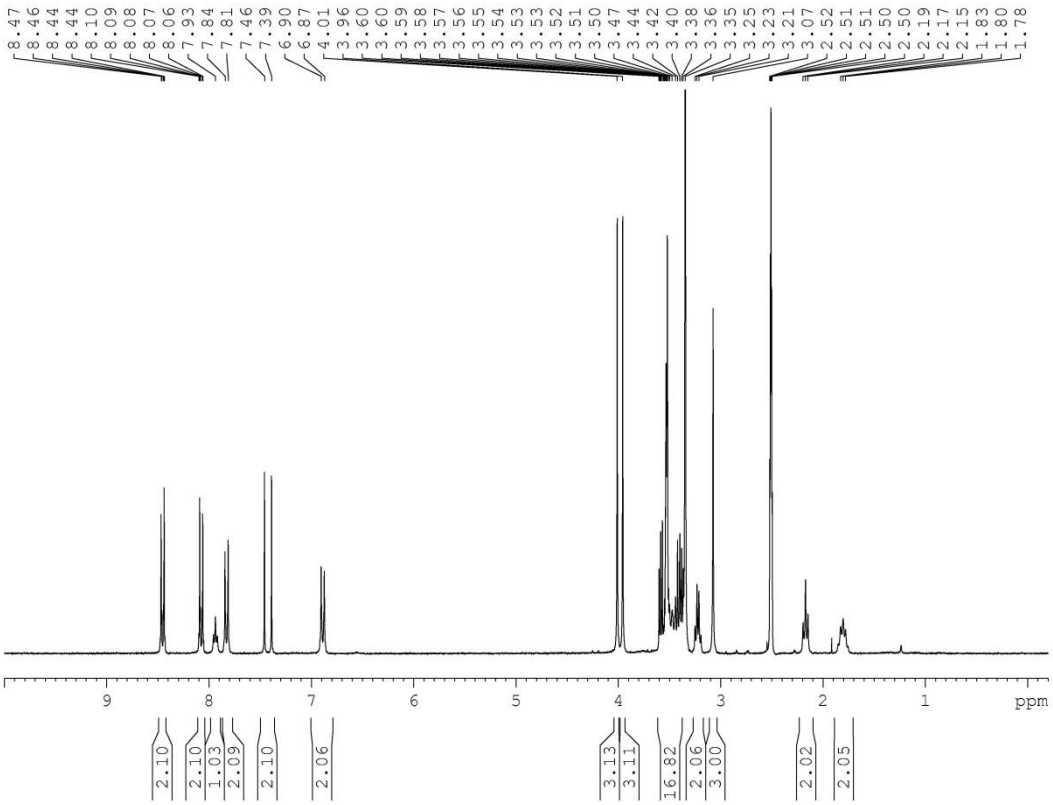

Figure S3. ^{1}H-NMR spectra of compound BHQ-2-N_3 in DMSO-d_6.

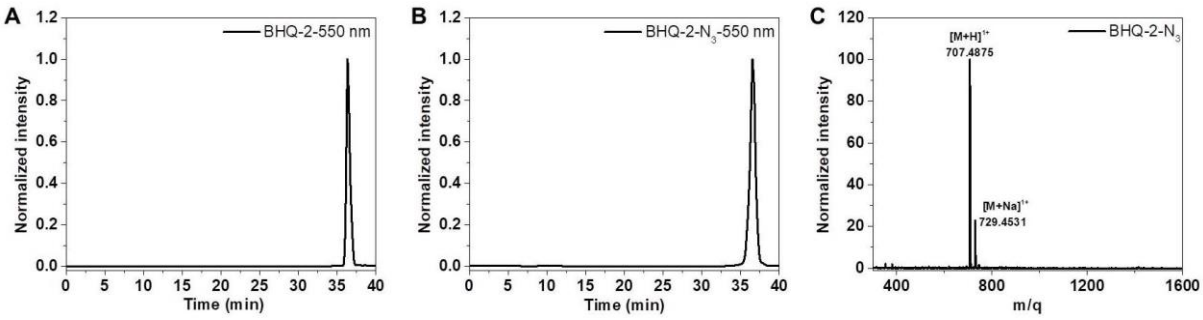

Figure S4. (A-B) High performance liquid chromatography (HPLC) results of compound BHQ-2 and BHQ-2-N_3, and (C) electrospray ionization mass spectrometry (ESI-MS) result of compound BHQ-2-N_3.

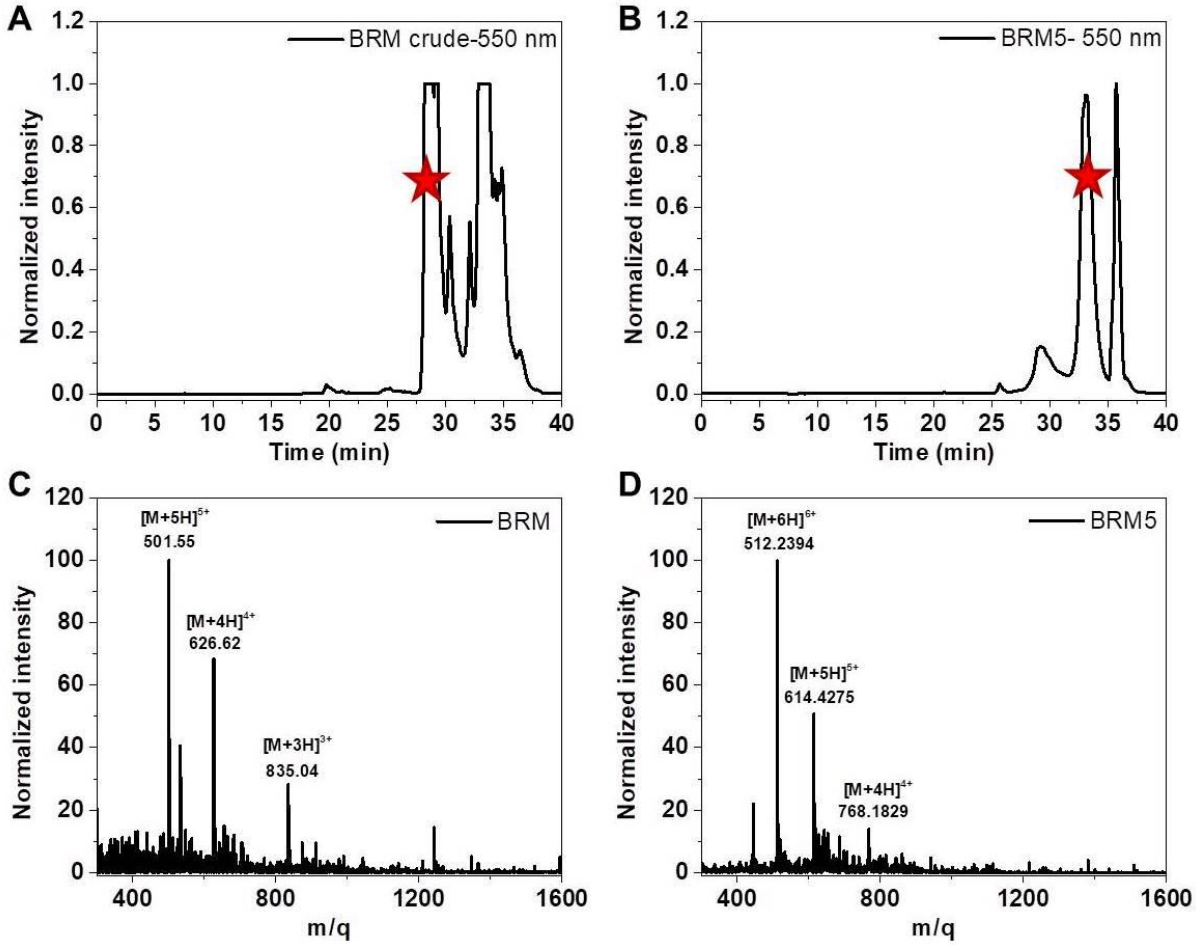

Figure S5. (A-B) HPLC and (C-D) ESI-MS results of compound BRM and BRM5. The red star represents the target product.

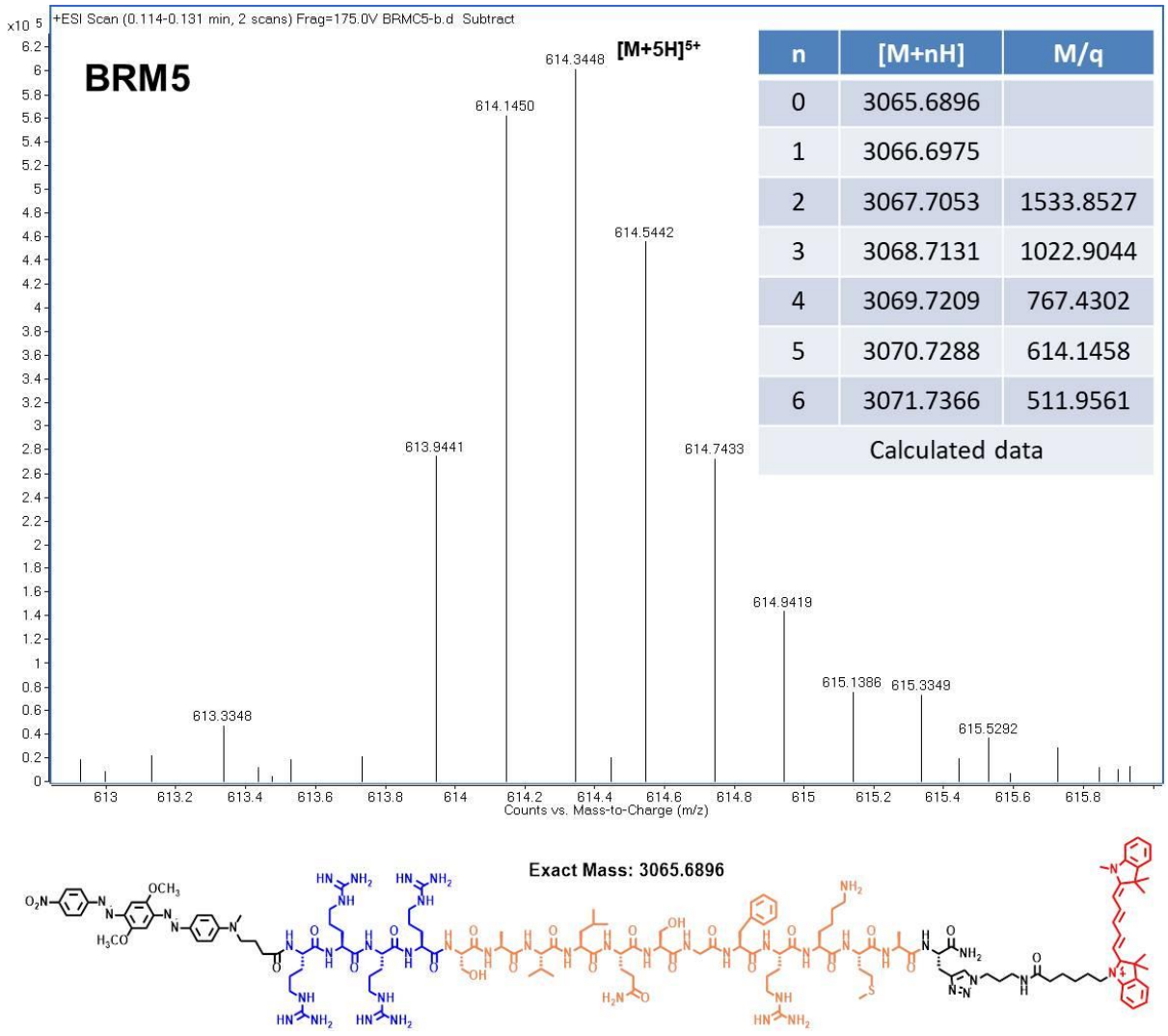

n	[M+nH]	M/q
0	3065.6896	
1	3066.6975	
2	3067.7053	1533.8527
3	3068.7131	1022.9044
4	3069.7209	767.4302
5	3070.7288	614.1458
6	3071.7366	511.9561
Calculated data		

Figure S6. High resolution mass spectra (HRMS) results of BRM5.

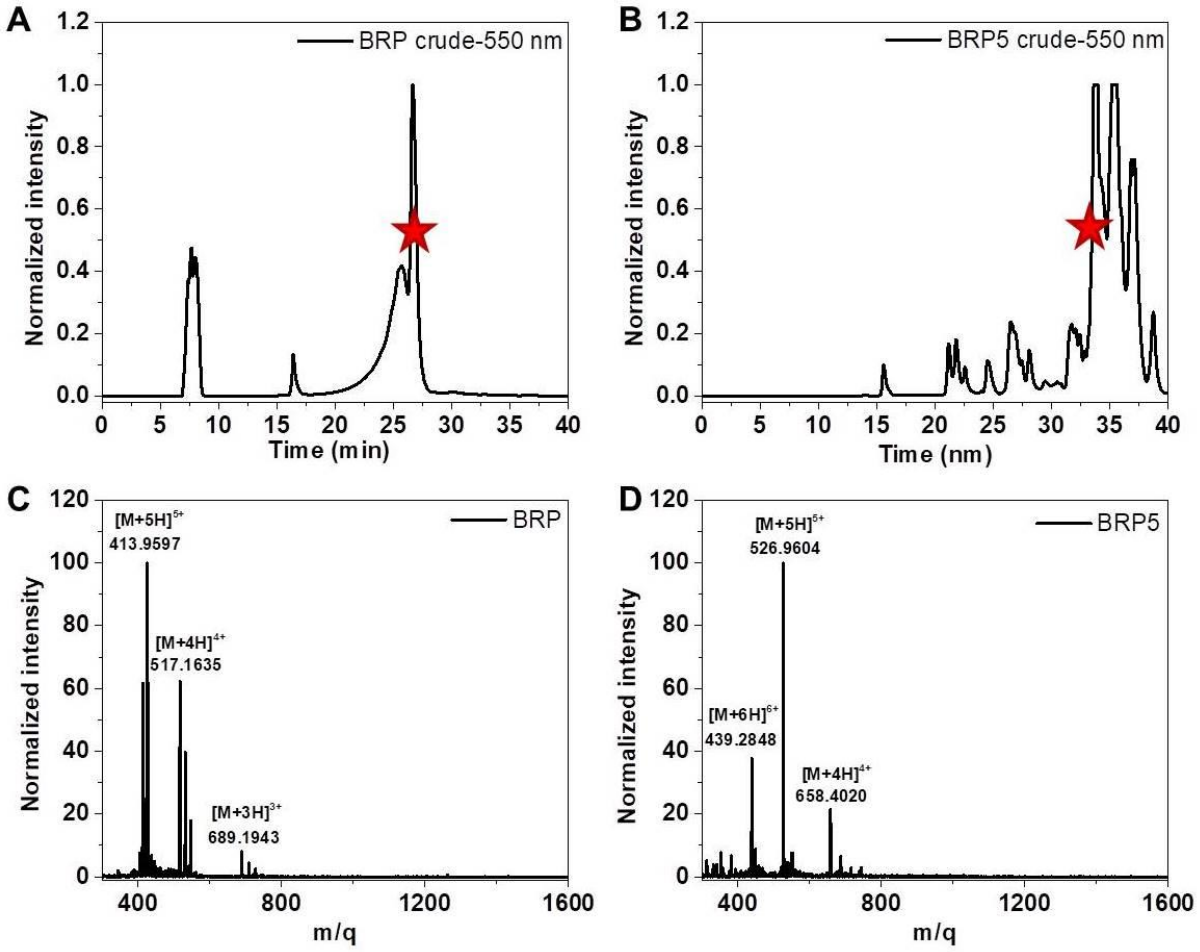

Figure S7. (A-B) HPLC and (C-D) ESI-MS results of compound BRP and BRP5. The red star represents the target product.

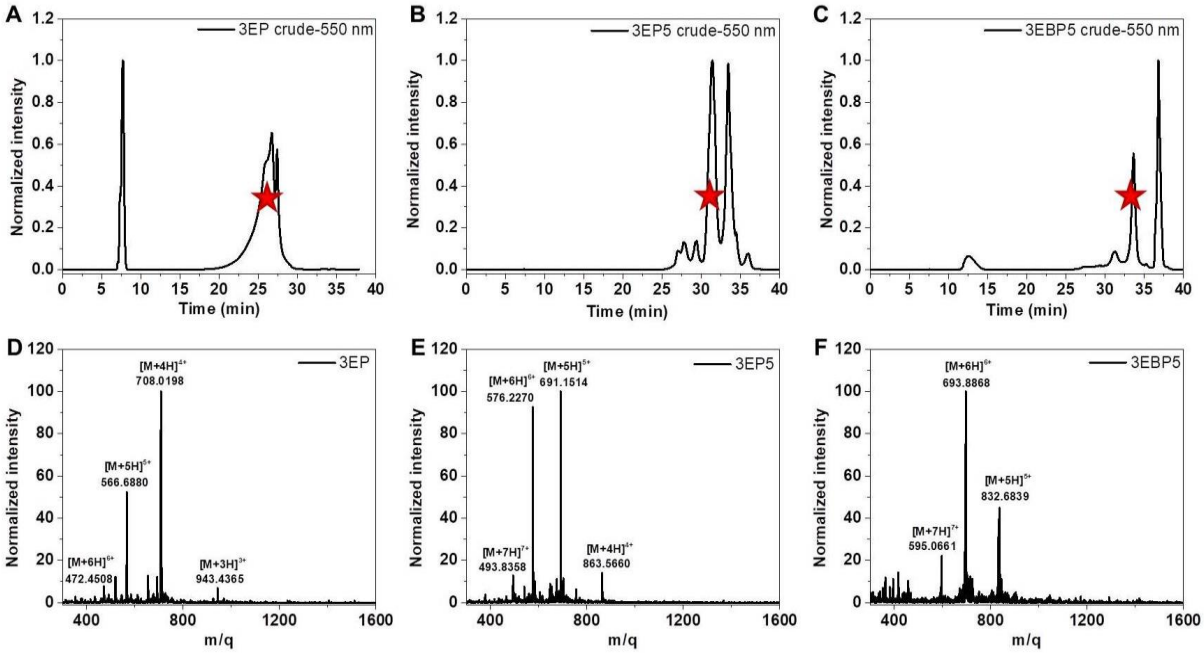

Figure S8. (A-C) HPLC and (D-F) ESI-MS results of compound 3EP, 3EP5, and 3EBP5.

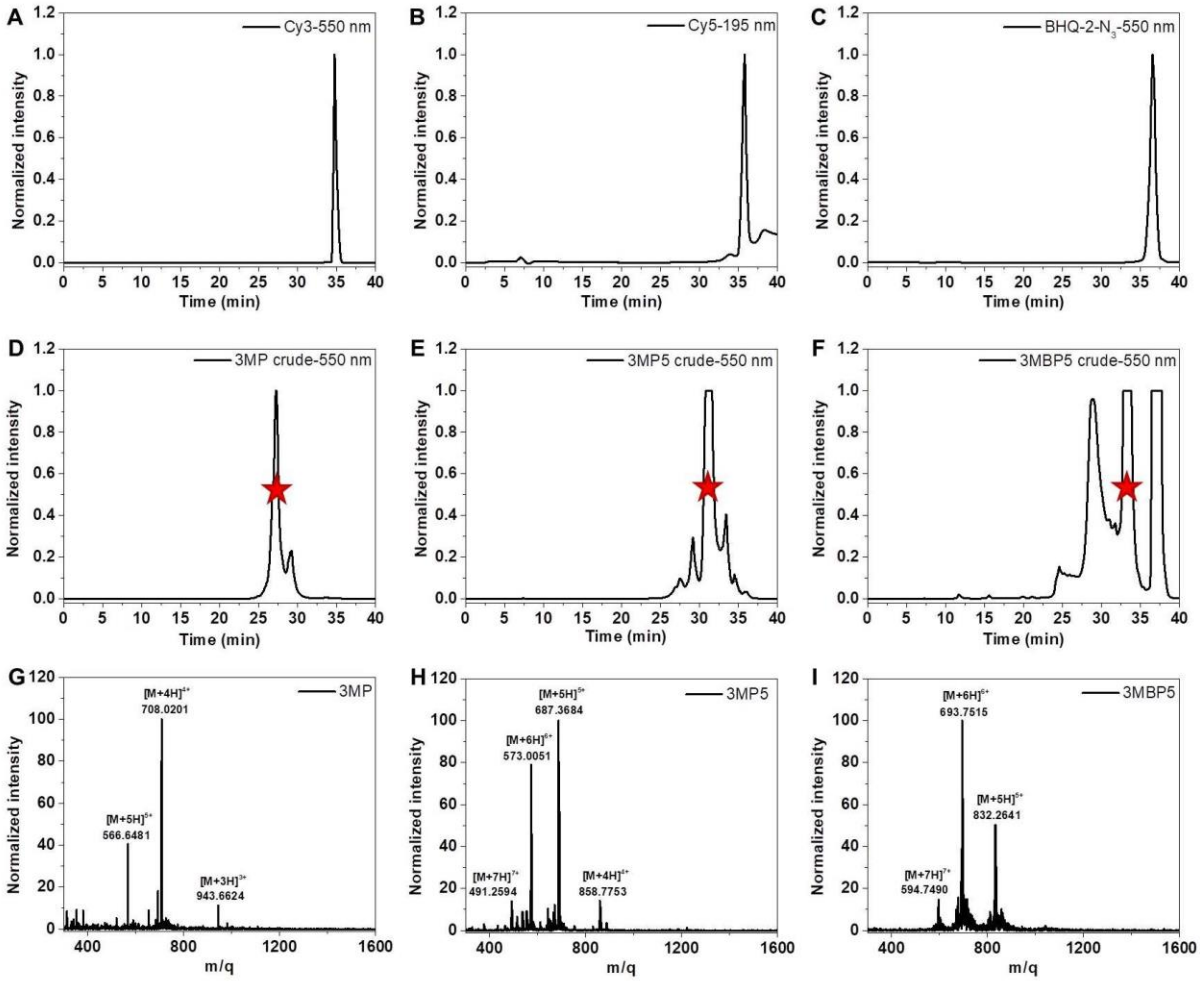

Figure S9. (A-F) HPLC results of Cy3, Cy5, BHQ-2-N_3, 3MP, 3MP5, and 3MBP5, and (G-I) ESI-MS results of compound 3MP, 3MP5 and 3MBP5. The red star represents the target product.

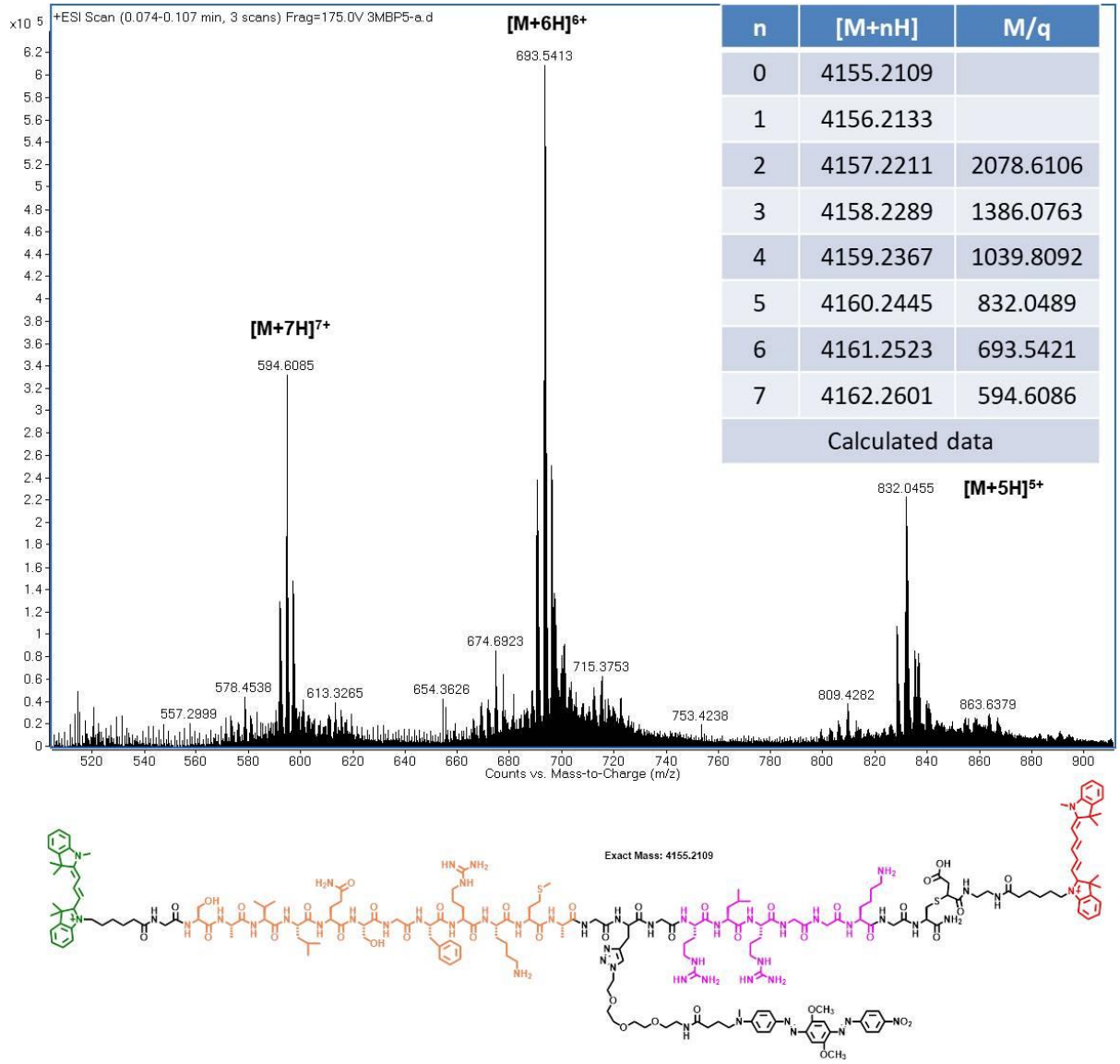

n	[M+nH]	M/q
0	4155.2109	
1	4156.2133	
2	4157.2211	2078.6106
3	4158.2289	1386.0763
4	4159.2367	1039.8092
5	4160.2445	832.0489
6	4161.2523	693.5421
7	4162.2601	594.6086
Calculated data		

Figure S10. HRMS results of 3MBP5.

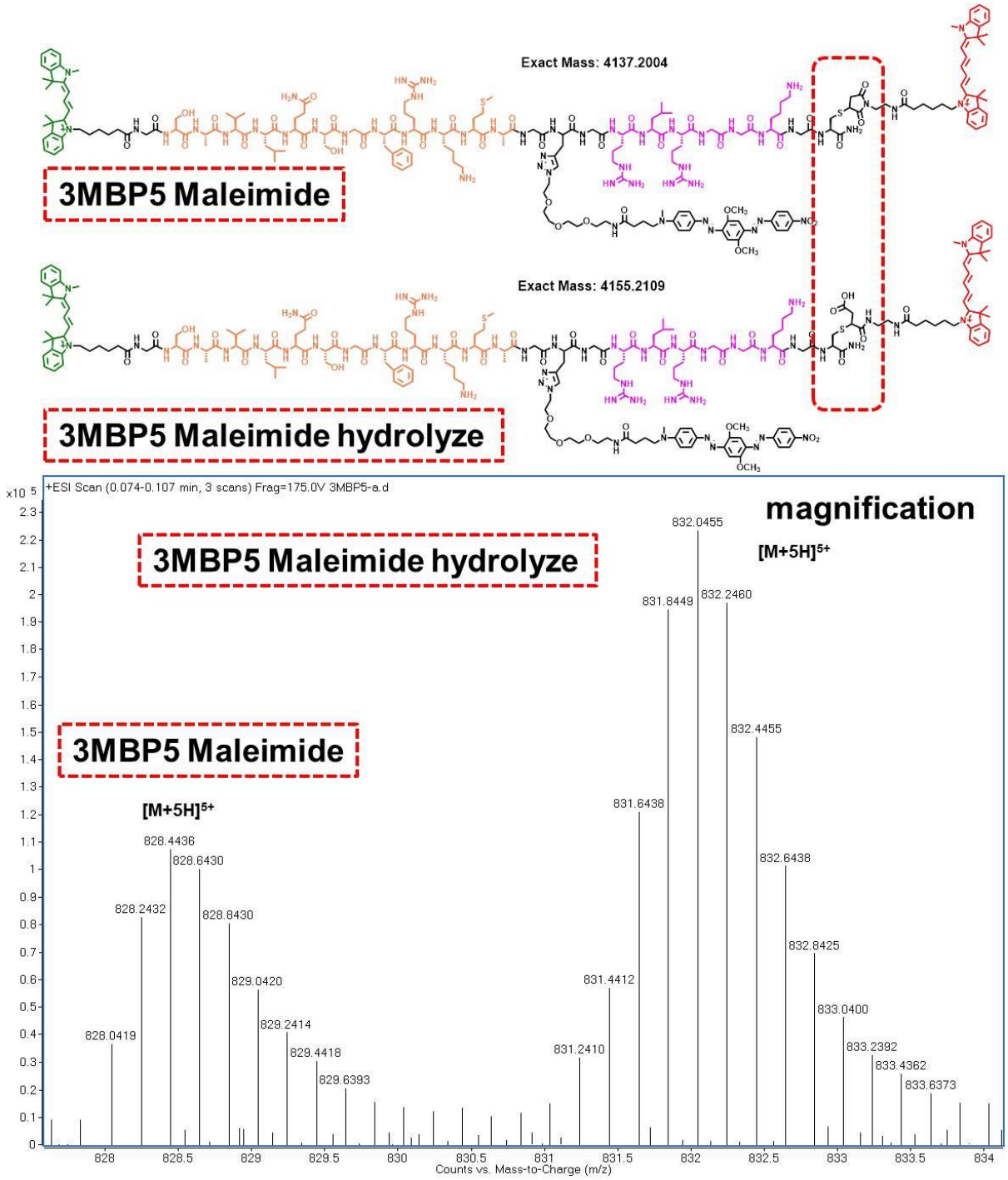

Figure S11. The magnification HRMS at $[M+5H]^{5+}$ results of 3MBP5.

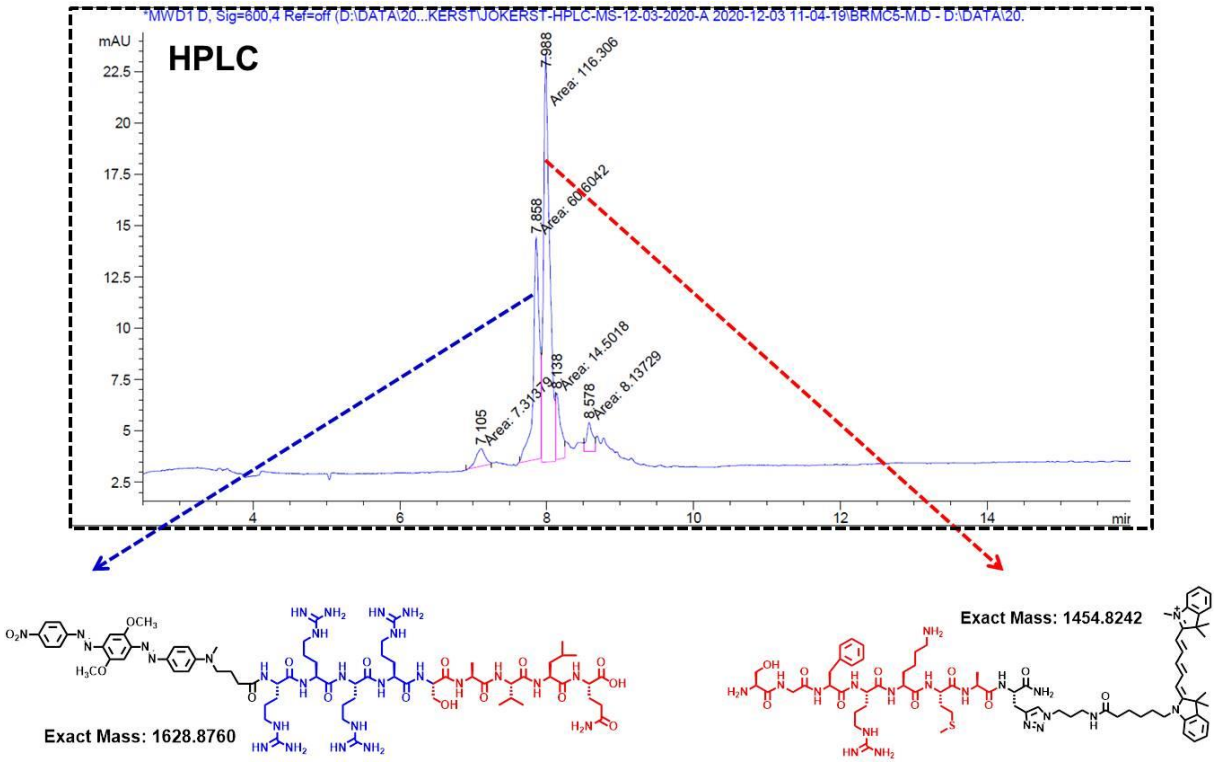

Figure S12. HPLC results showed that compound BRM5 was cleaved by M^{pro}.

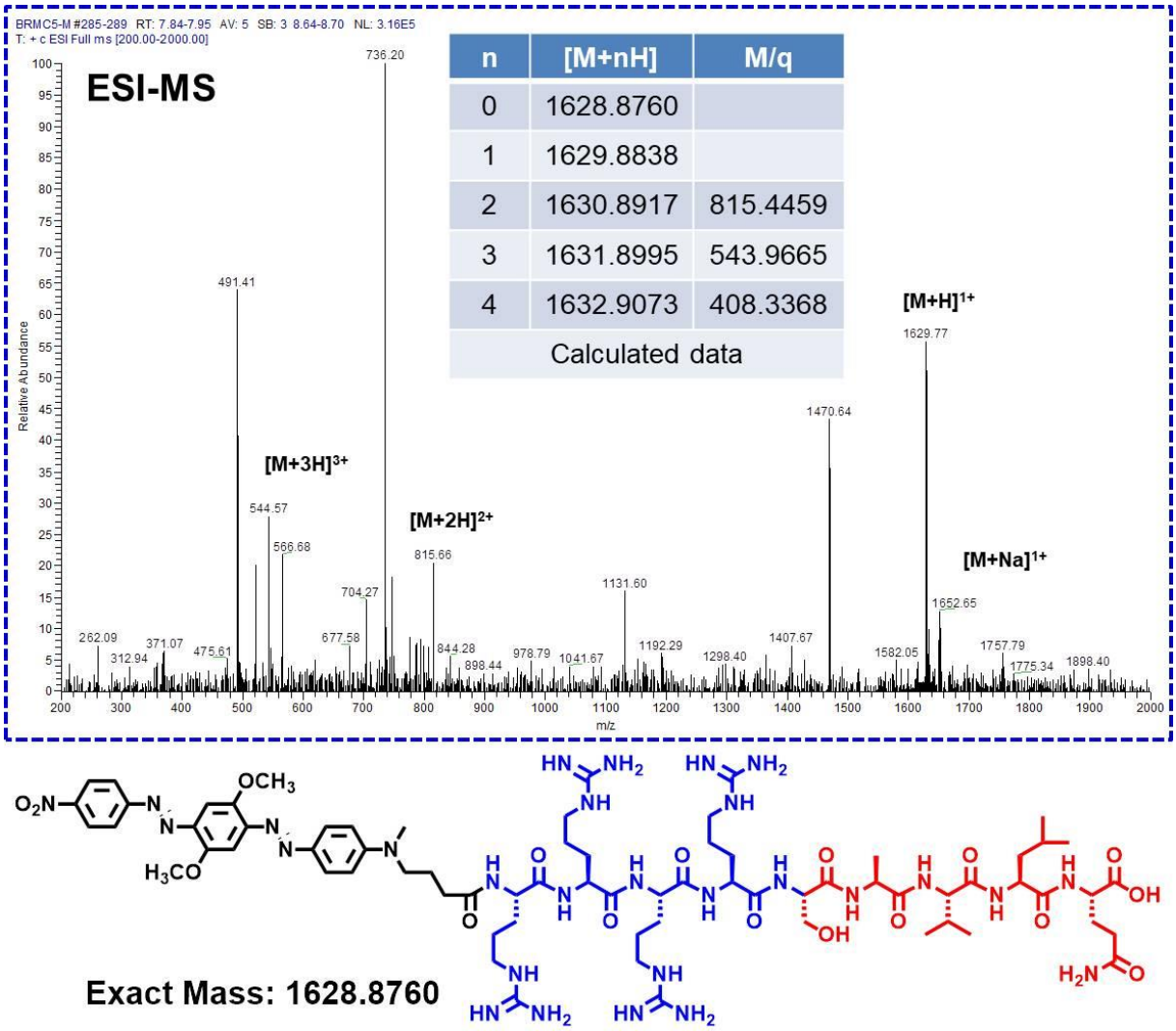

Figure S13. ESI-MS results showed that compound BRM5 was cleaved by M^{pro} (N-terminal).

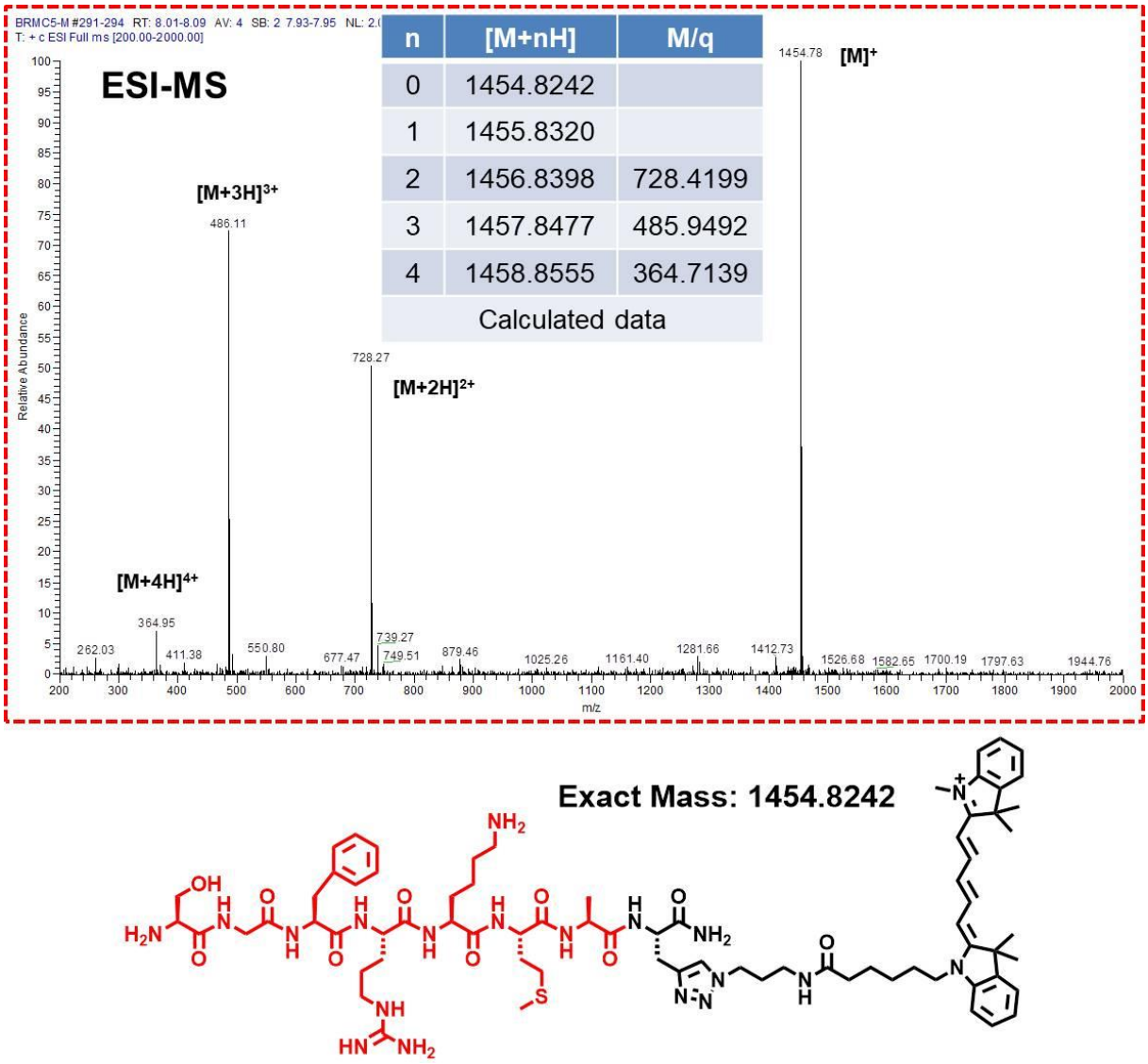

Figure S14. ESI-MS results showed that compound BRM5 was cleaved by M^{pro} (C-terminal).

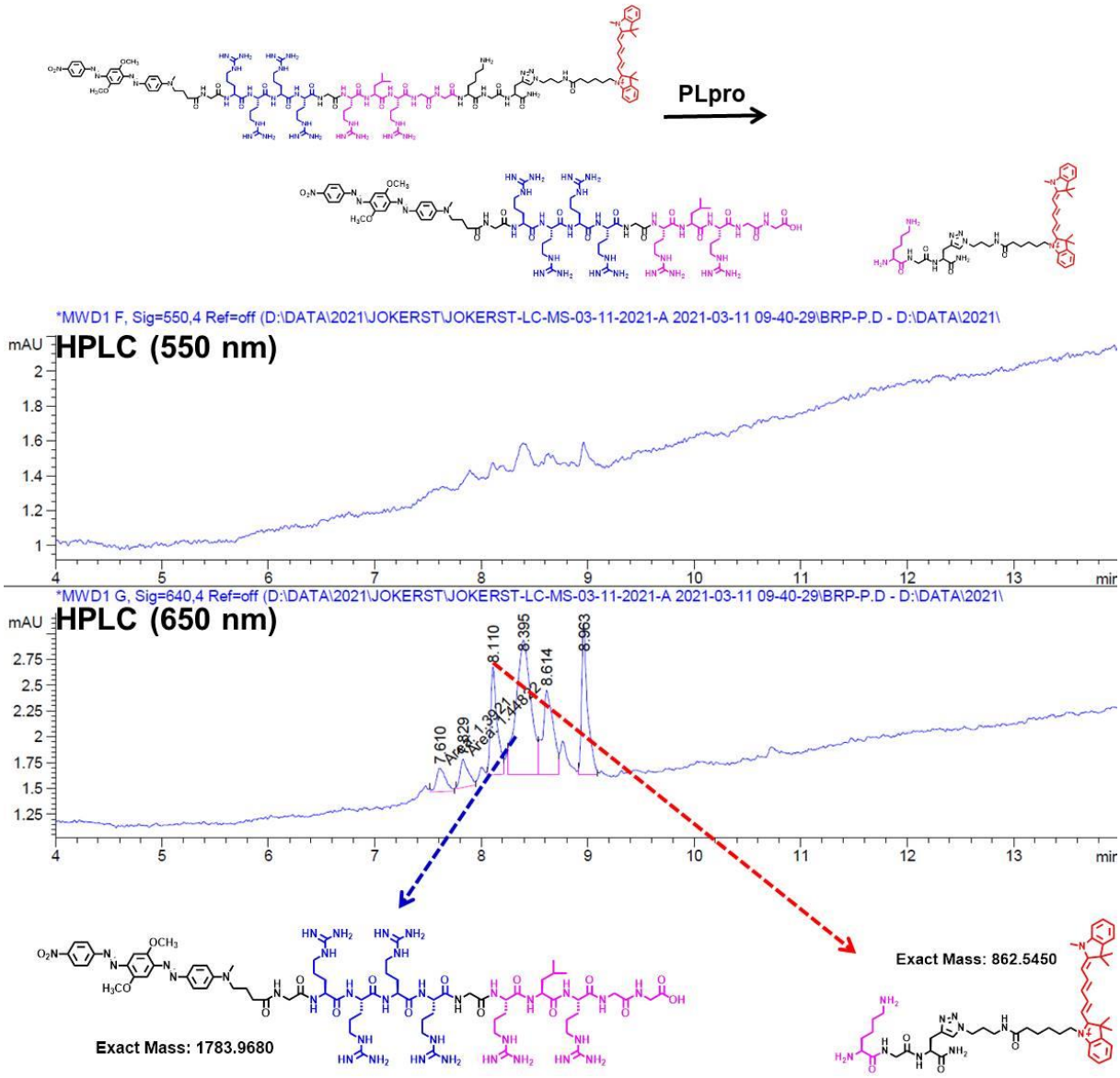

Figure S15. HPLC results showed that compound BRP5 was cleaved by PL^{pro}.

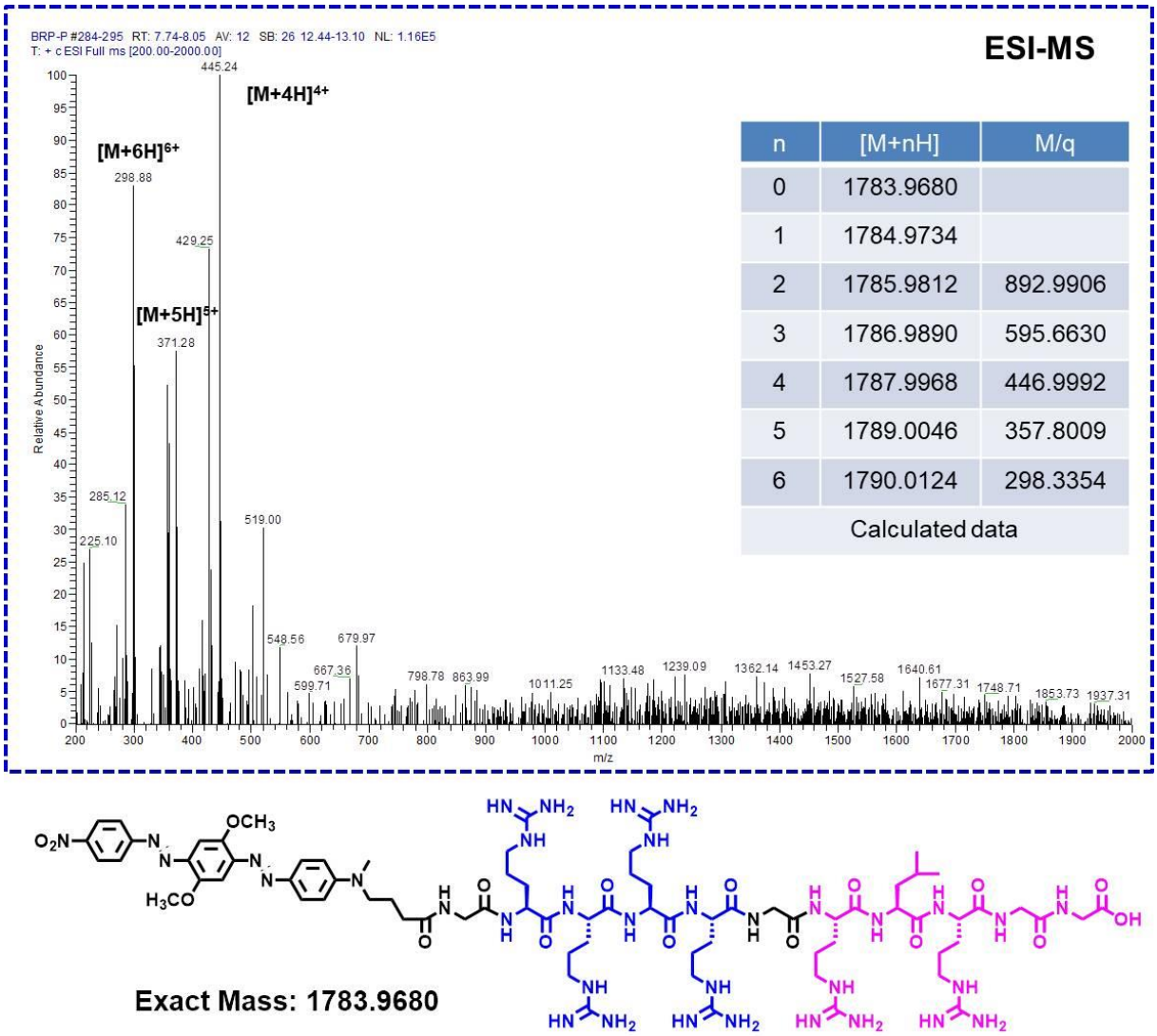

n	[M+nH]	M/q
0	1783.9680	
1	1784.9734	
2	1785.9812	892.9906
3	1786.9890	595.6630
4	1787.9968	446.9992
5	1789.0046	357.8009
6	1790.0124	298.3354
Calculated data		

Figure S16. ESI-MS results showed that compound BRP5 was cleaved by PL^{pro} (N-terminal).

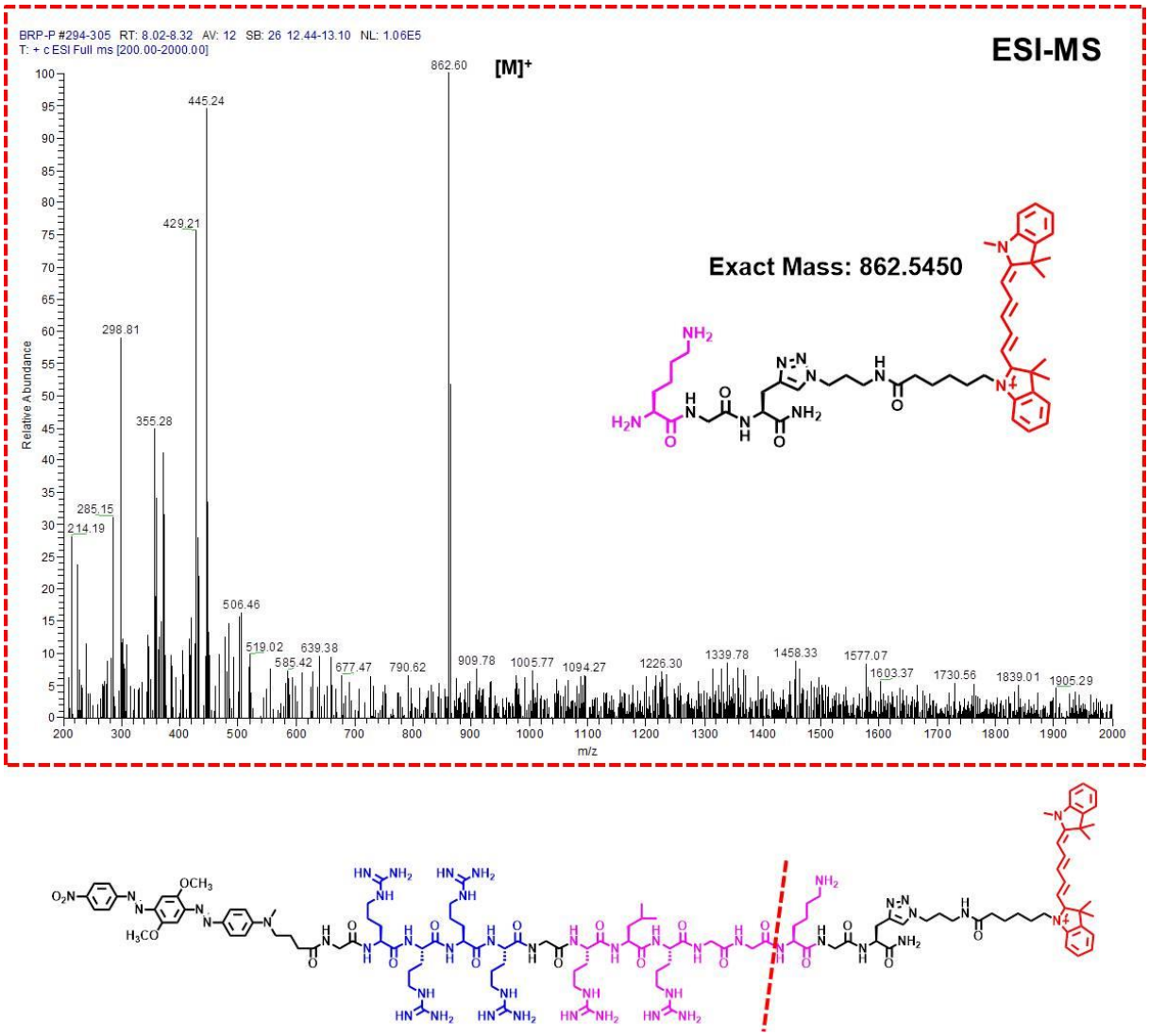

Figure S17. ESI-MS results showed that compound BRP5 was cleaved by PL^{pro} (C-terminal).

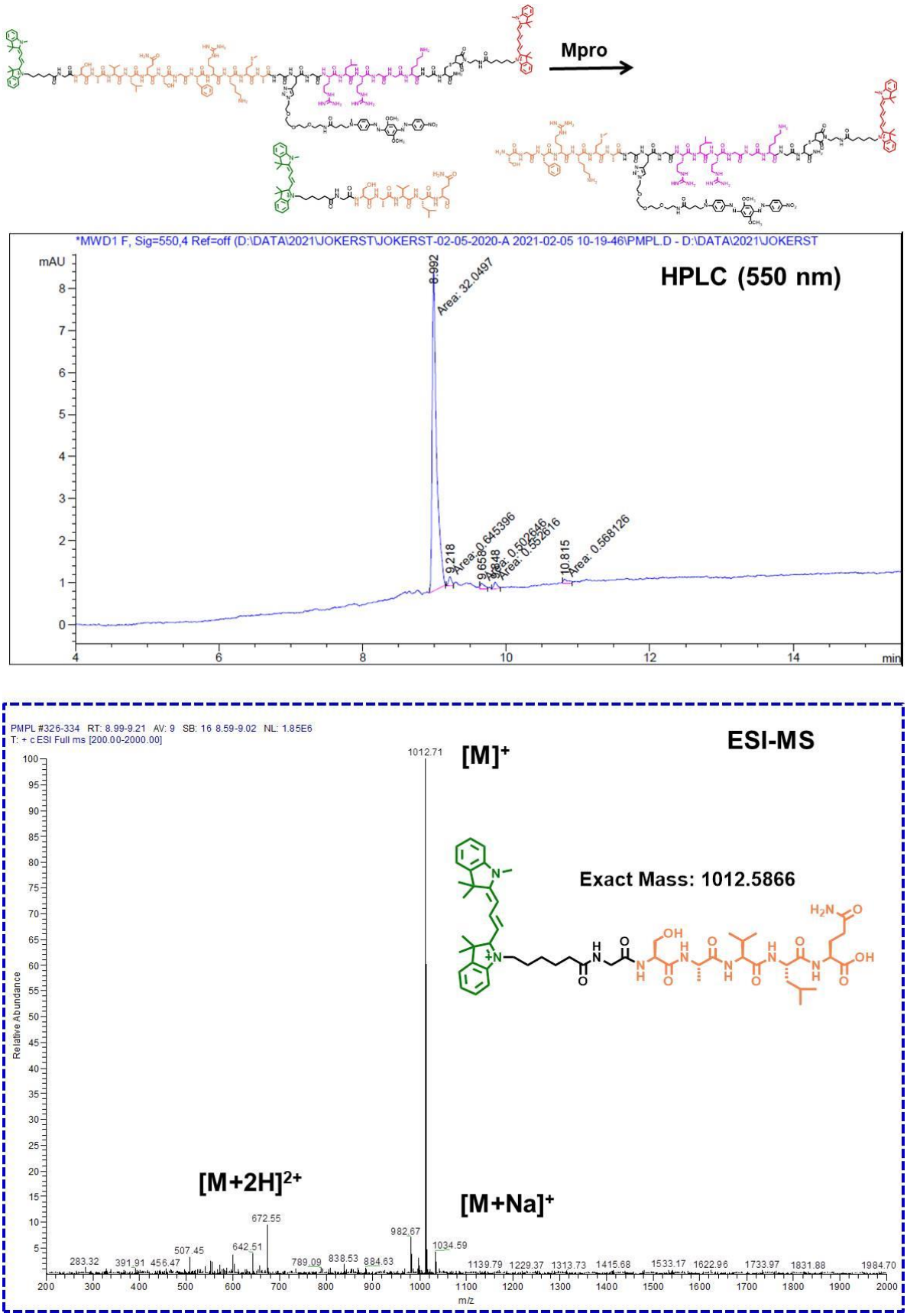

Figure S18. HPLC-MS results showed that compound 3MBP5 was cleaved by M^{pro}.

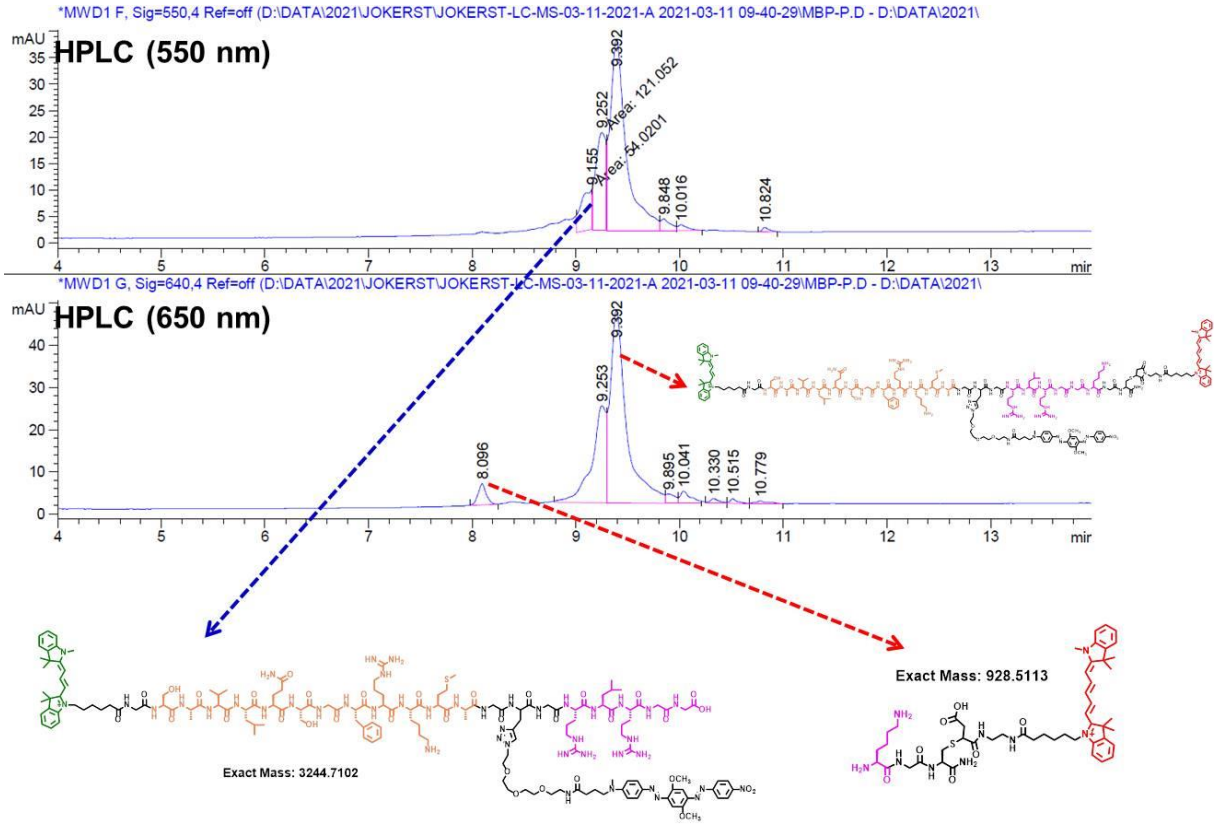

Figure S19. HPLC results showed that compound 3MBP5 was cleaved by PL^{pro}.

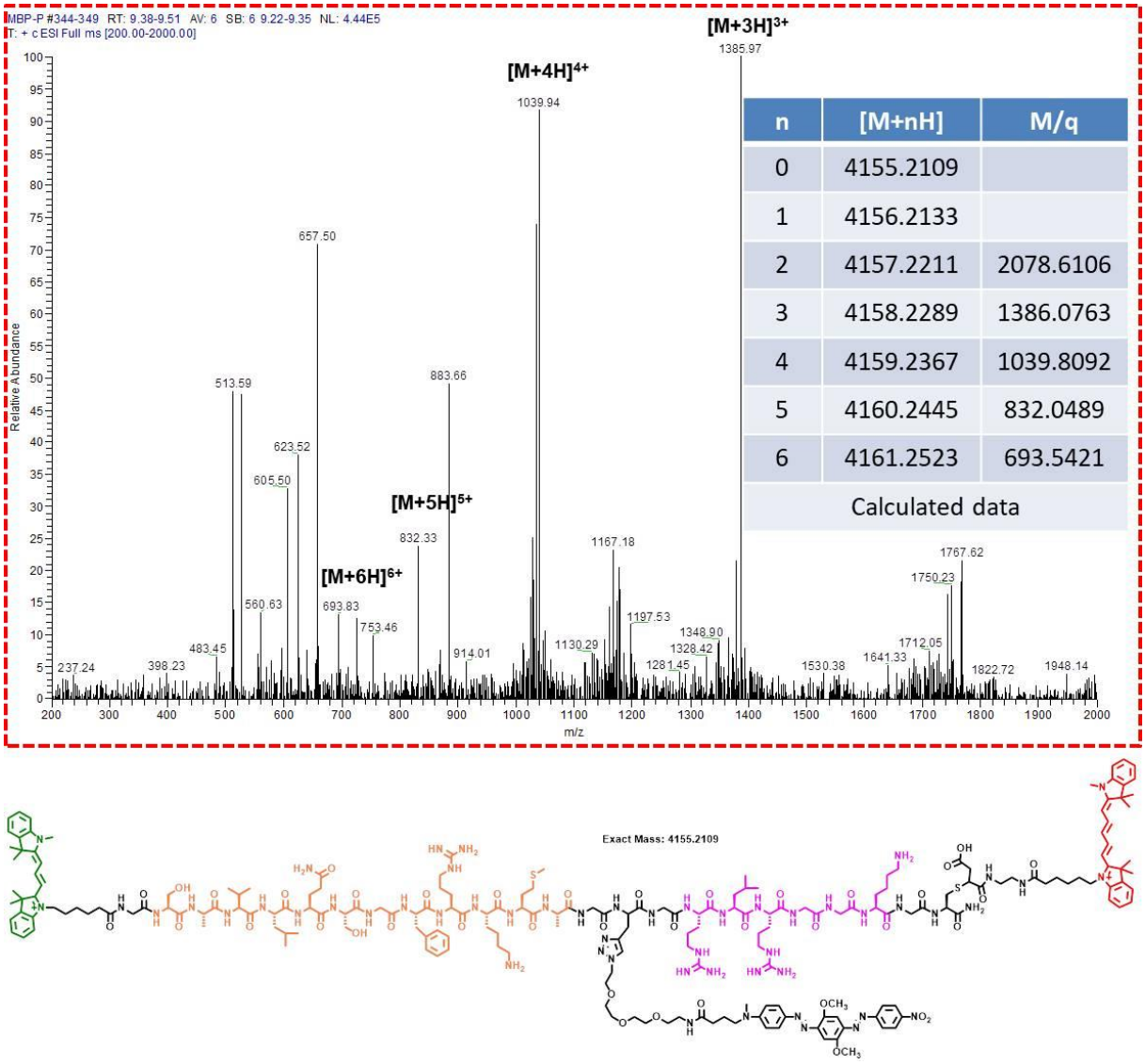

n	[M+nH]	M/q
0	4155.2109	
1	4156.2133	
2	4157.2211	2078.6106
3	4158.2289	1386.0763
4	4159.2367	1039.8092
5	4160.2445	832.0489
6	4161.2523	693.5421
Calculated data		

Figure S20. ESI-MS results showed that some of compound 3MBP5 did not be cleaved by PL^{pro}.

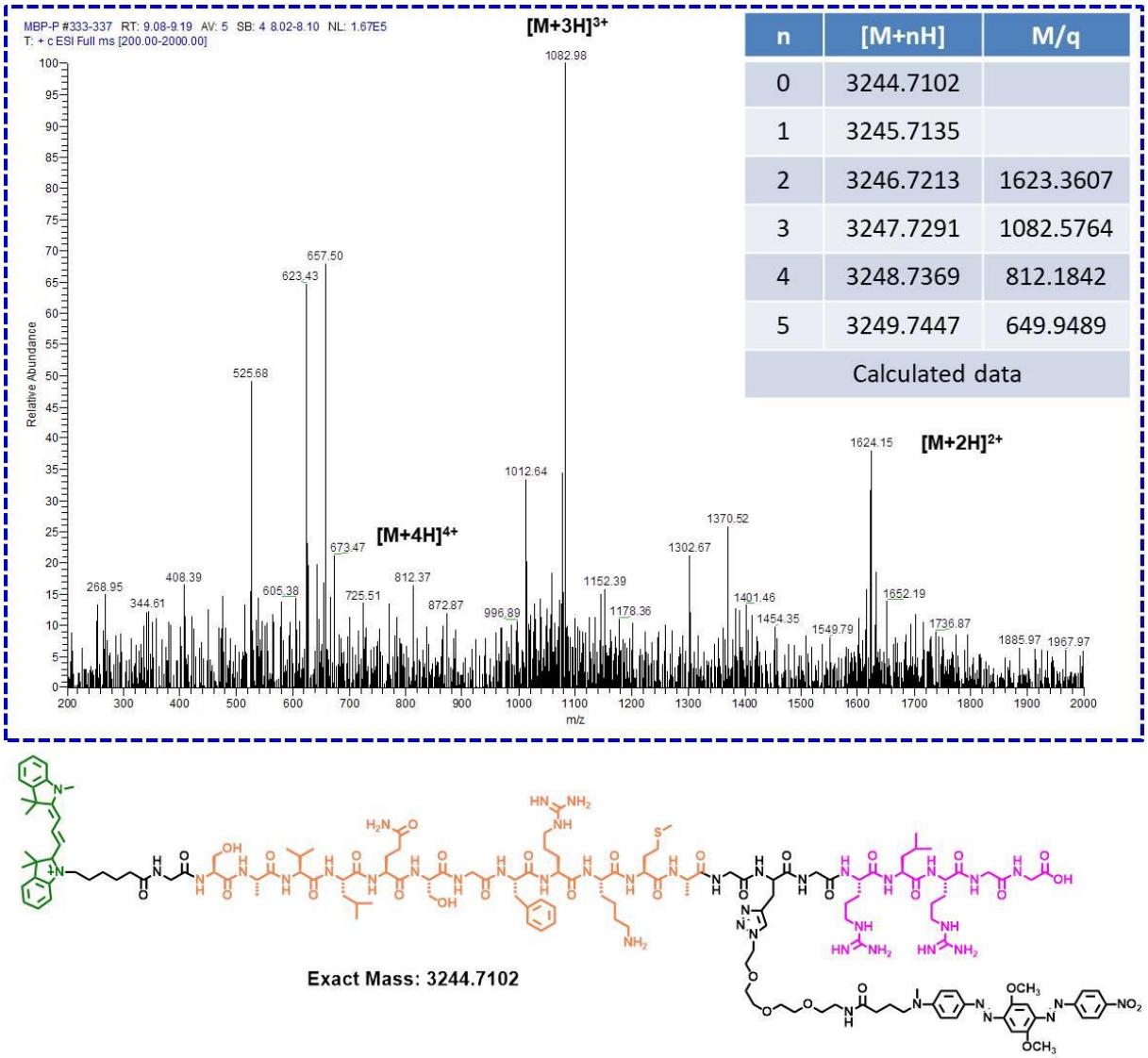

n	[M+nH]	M/q
0	3244.7102	
1	3245.7135	
2	3246.7213	1623.3607
3	3247.7291	1082.5764
4	3248.7369	812.1842
5	3249.7447	649.9489
Calculated data		

Figure S21. ESI-MS results showed that compound 3MBP5 was cleaved by PL^{pro} (N-terminal).

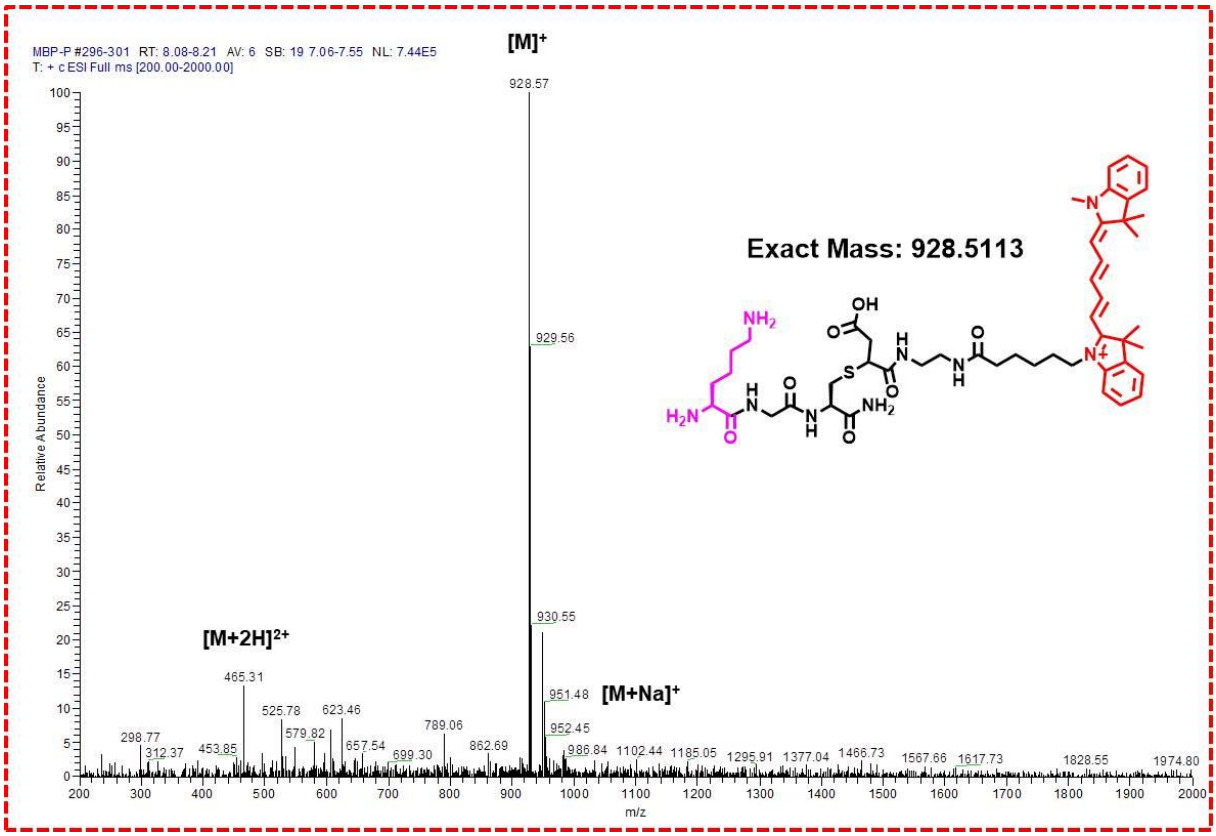

Figure S22. ESI-MS results showed that compound 3MBP5 was cleaved by PL^{pro} (C-terminal).

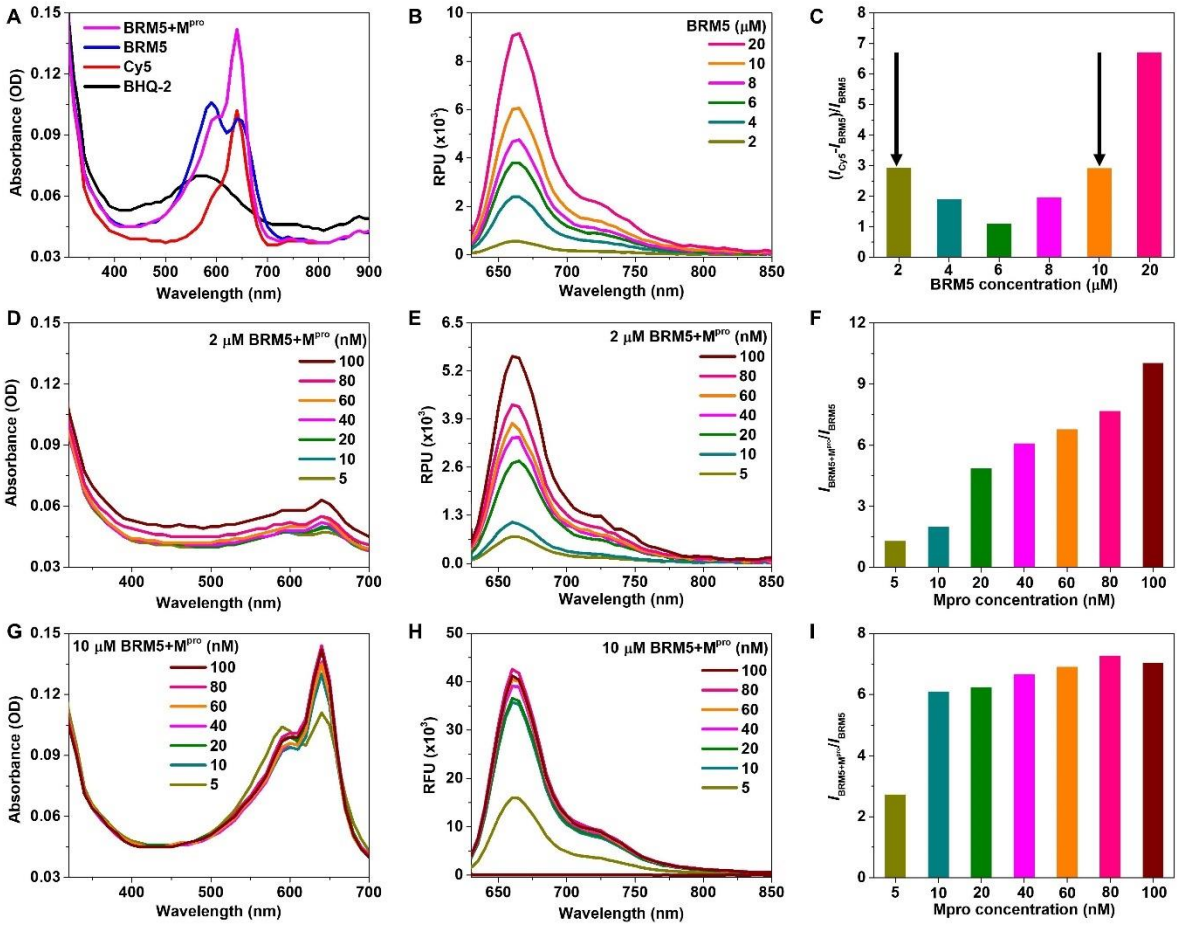

Figure S23. (A) UV−vis absorption of 10.0 μM BHQ-2, 10.0 μM Cy5, 10.0 μM BRM5 in Tris-HCl buffer with 1% (v/v) DMSO and 10.0 μM BRM5 after incubation with 100 nM M^{pro} at 37 ^{0}C for 1 h. (B) Fluorescence spectra of 2.0 μM, 4.0 μM, 6.0 μM, 8.0 μM, 10.0 μM and 20.0 μM BRM5 in Tris-HCl buffer with 1% (v/v) DMSO. (C) Plot of $(I_{Cy5}-I_{BRM5})/I_{BRM5}$ versus the related fluorescence intensity of (2.0 μM, 4.0 μM, 6.0 μM, 8.0 μM, 10.0 μM, 20.0 μM) Cy5 and (2.0 μM, 4.0 μM, 6.0 μM, 8.0 μM, 10.0 μM, 20.0 μM) BRM5 under the excitation wavelength of 600 nm. (D) UV−vis absorption, (E) fluorescence spectra and (F) plot of $I_{BRM5+M^{pro}}/I_{BRM5}$ versus the related fluorescence intensity of 2.0 μM BRM5 after incubation with (5 nM, 10 nM, 20 nM, 40 nM, 60 nM, 80 nM, and 100 nM) M^{pro} under the excitation wavelength of 600 nm. (G) UV−vis absorption, (H) fluorescence spectra and (I) plot of $I_{BRM5+M^{pro}}/I_{BRM5}$ versus the related fluorescence intensity of 10.0 μM BRM5 after incubation with (5 nM, 10 nM, 20 nM, 40 nM, 60 nM, 80 nM, and 100 nM) M^{pro} under an excitation wavelength of 600 nm.

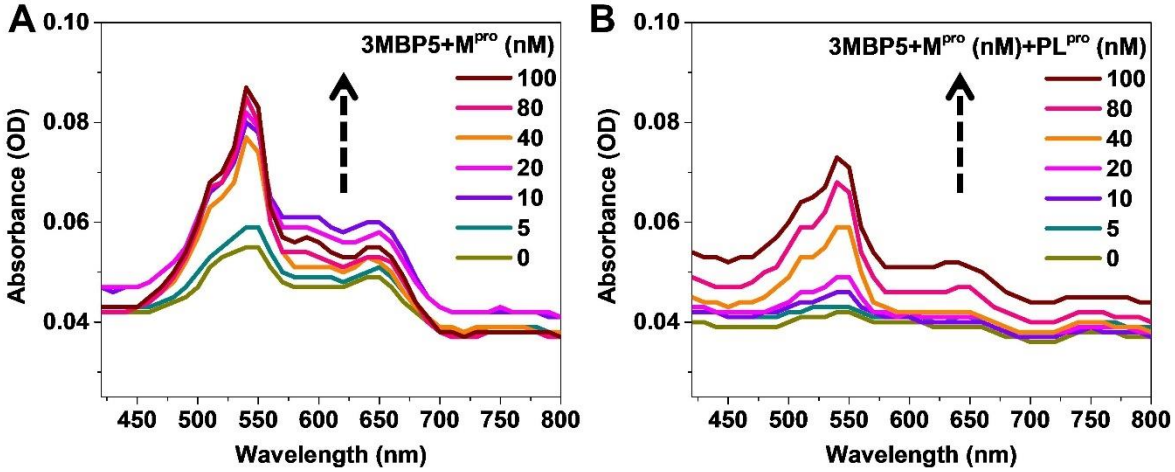

Figure S24. UV−vis absorption spectra of 2.0 μM 3MBP5 after incubation with different concentrations of (A) M^{pro}, (B) M^{pro} and PL^{pro} at 37 ^{0}C for 1 h.

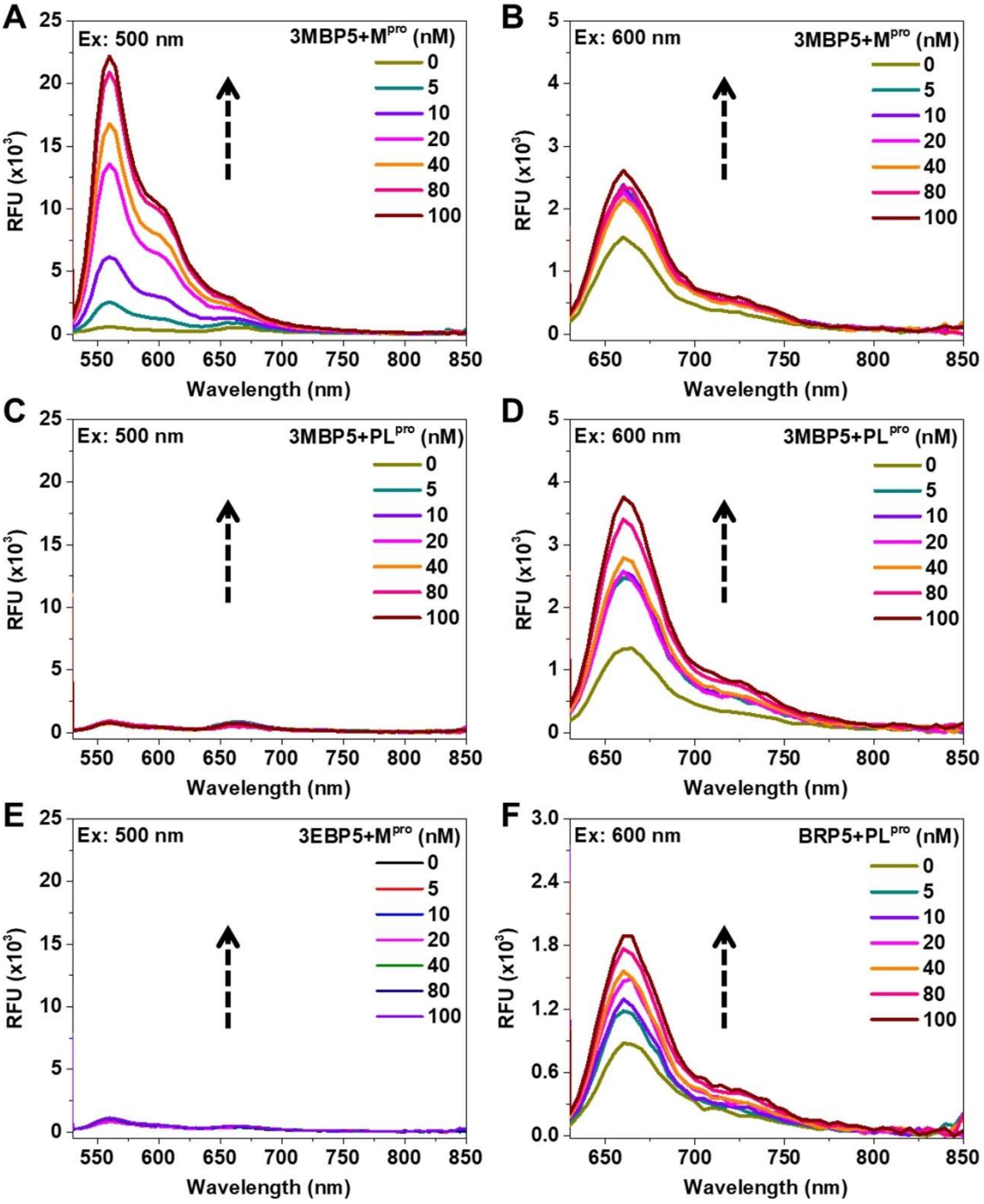

Figure S25. Fluorescence spectra of 2.0 μM 3MBP5, 2.0 μM 3EBP5 and 2.0 μM BRP5 after incubation with different concentration of M^{pro} and PL^{pro} in Tris-HCl buffer for 1 h under the excitation wavelength of 500 nm or 600 nm. (A-B) 3MBP5 with M^{pro}, (C-D) 3MBP5 with PL^{pro}, (E) 3EBP5 with M^{pro}, and (F) BRP5 with PL^{pro}.

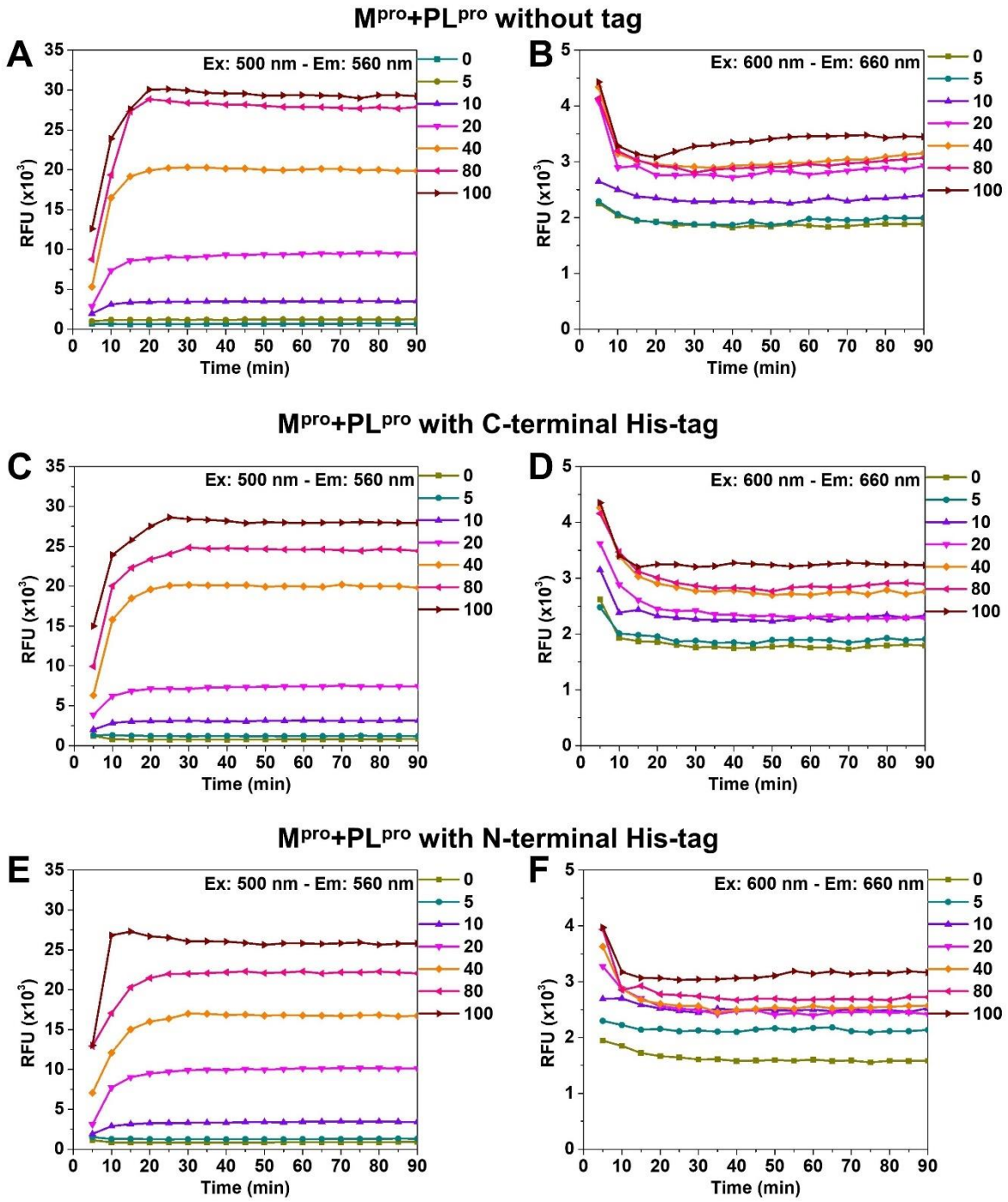

Figure S26. Time-dependent fluorescence spectra of 2 μM 3MBP5 incubation with 5 nM, 10 nM, 20 nM, 40 nM, 80 nM, and 100 nM M^{pro} and PL^{pro} without tag (A-B), PL^{pro} with C-termnal His-tag (C-D), and PL^{pro} with N-terminal His-tag (E-F) in Tris-HCl buffer for 90 mins under an excitation wavelength of 500 nm or 600 nm.

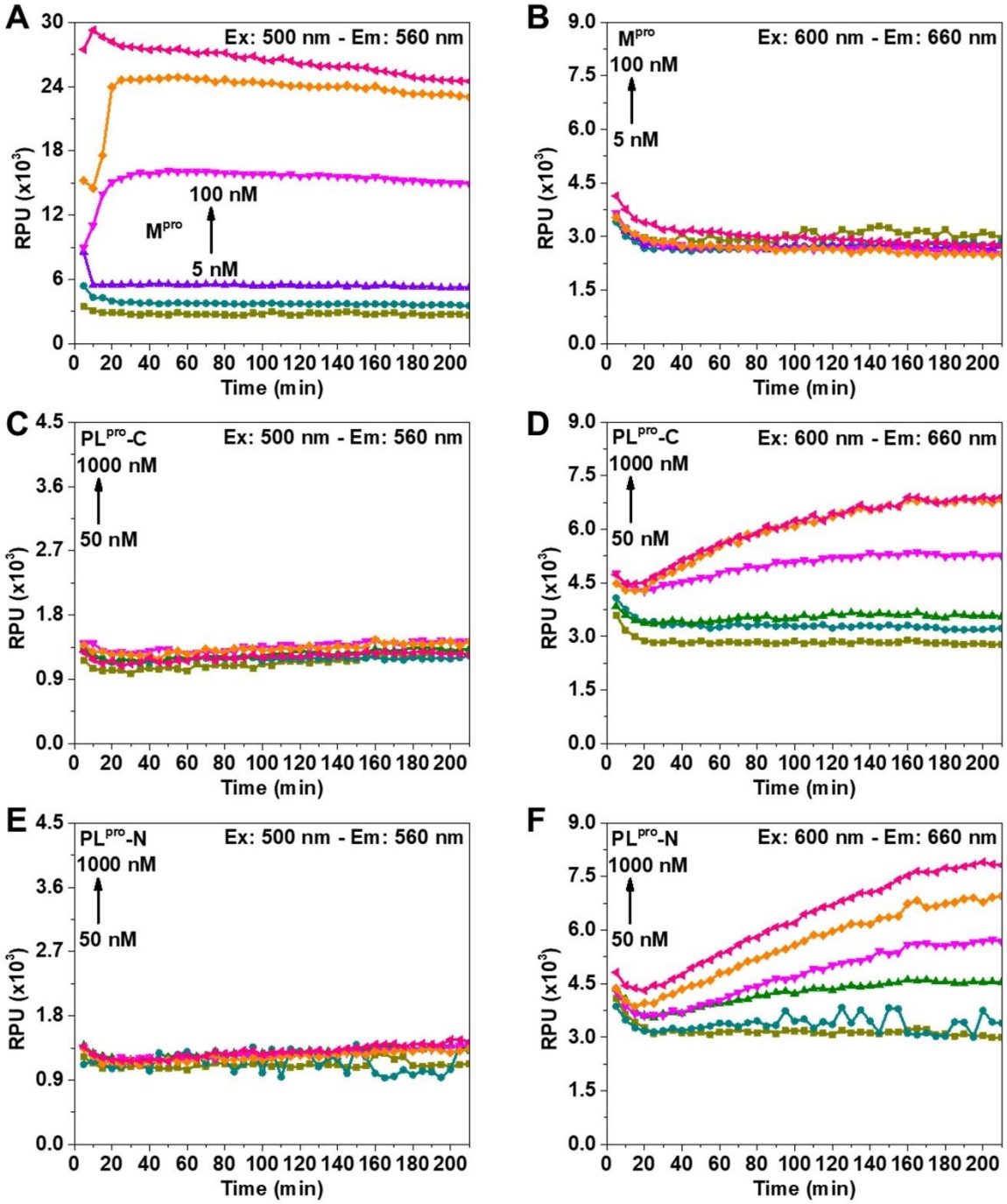

Figure S27. Time-dependent fluorescence spectra of 2 μM 3MBP5 incubation with (A-B) 5 nM, 10 nM, 20 nM, 40 nM, 80 nM and 100 nM M^{pro}, (C-D) 50 nM, 100 nM, 200 nM, 400 nM, 800 nM and 1000 nM PL^{pro} with C-termnal His-tag, or (E-F) 50 nM, 100 nM, 200 nM, 400 nM, 800 nM and 1000 nM PL^{pro} with N-terminal His-tag in Tris-HCl buffer for 210 mins under the excitation wavelength of 500 nm or 600 nm. The PL^{pro}-C represents PL^{pro} with C-termnal His-tag. The PL^{pro}-N represents PL^{pro} with N-termnal His-tag.

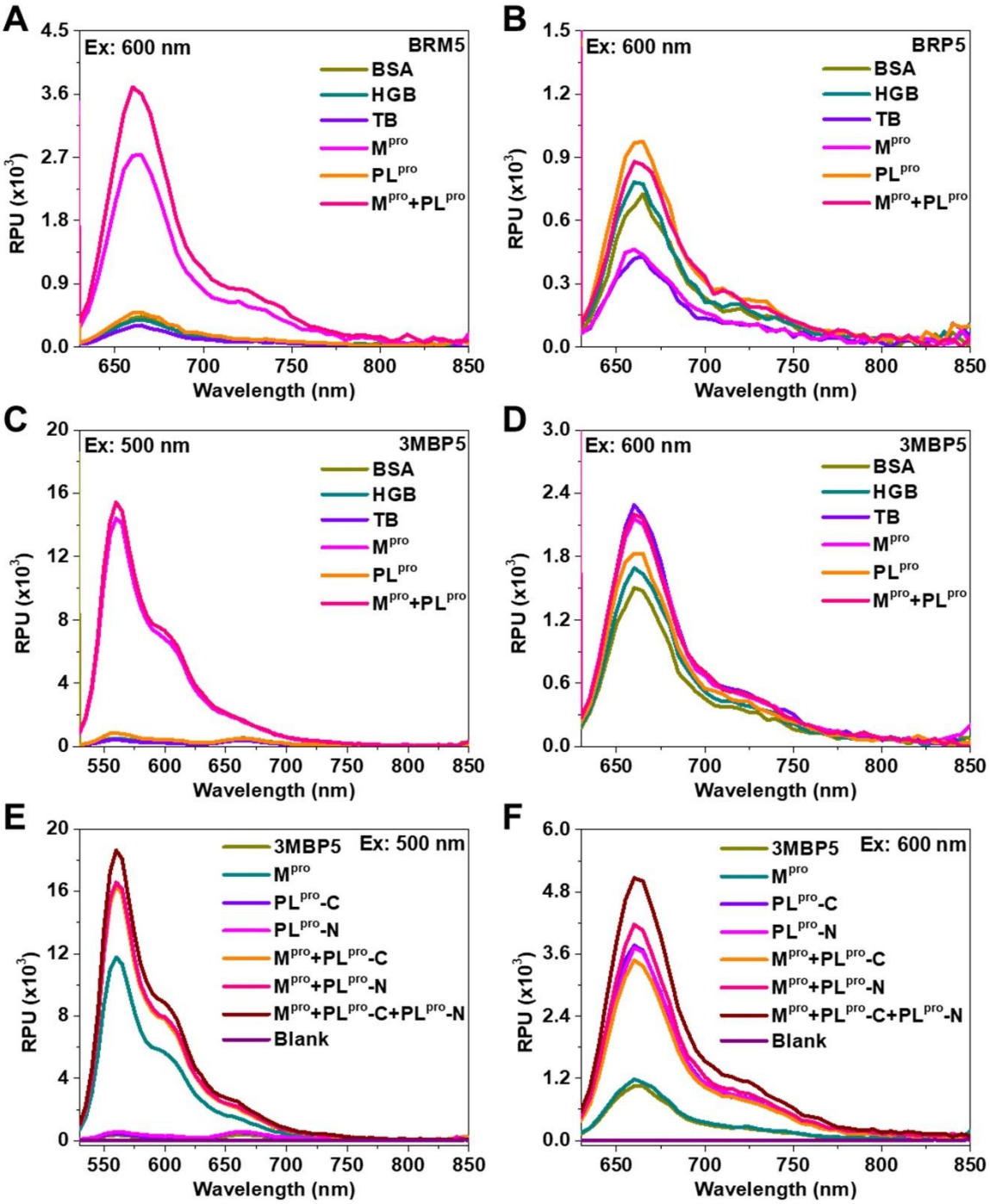

Figure S28. Fluorescence spectra of 2.0 μM BRM5, 2.0 μM BRP5, and 2.0 μM 3MBP5 after incubation with different kinds of proteases in Tris-HCl buffer for 1 h under the excitation wavelength of 500 nm or 600 nm. (A) BRM5 was incubated with 100 nM different kinds of proteases. (B) BRP5 was incubated with 100 nM different kinds of proteases. (C-D) 3MBP5 was incubated with 100 nM different kinds of proteases. (E-F) 3MBP5 was incubated with 100 nM M^{pro} or/and 1000 nM different kinds of PL^{pro}. The PL^{pro}-C represents PL^{pro} with C-termnal His-tag. The PL^{pro}-N represents PL^{pro} with N-termnal His-tag.

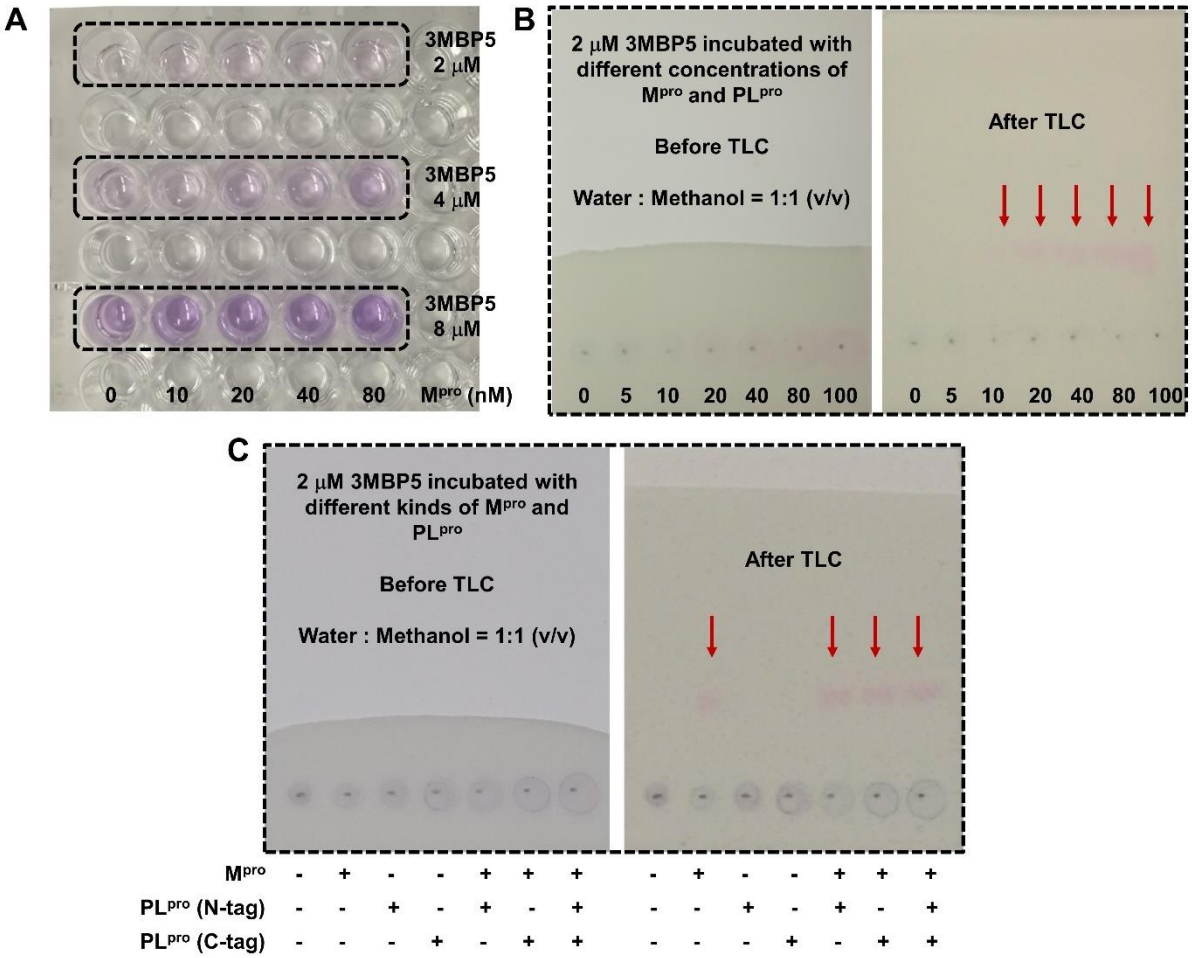

Figure S29. Photographs of 3MBP5 incubation with different concentrations of (A) M^{pro}, (B) M^{pro} and PL^{pro}, and (C) 100 nM M^{pro} and different kinds of 1000 nM PL^{pro} at room temperature for (25 ^{0}C) for 1 h.

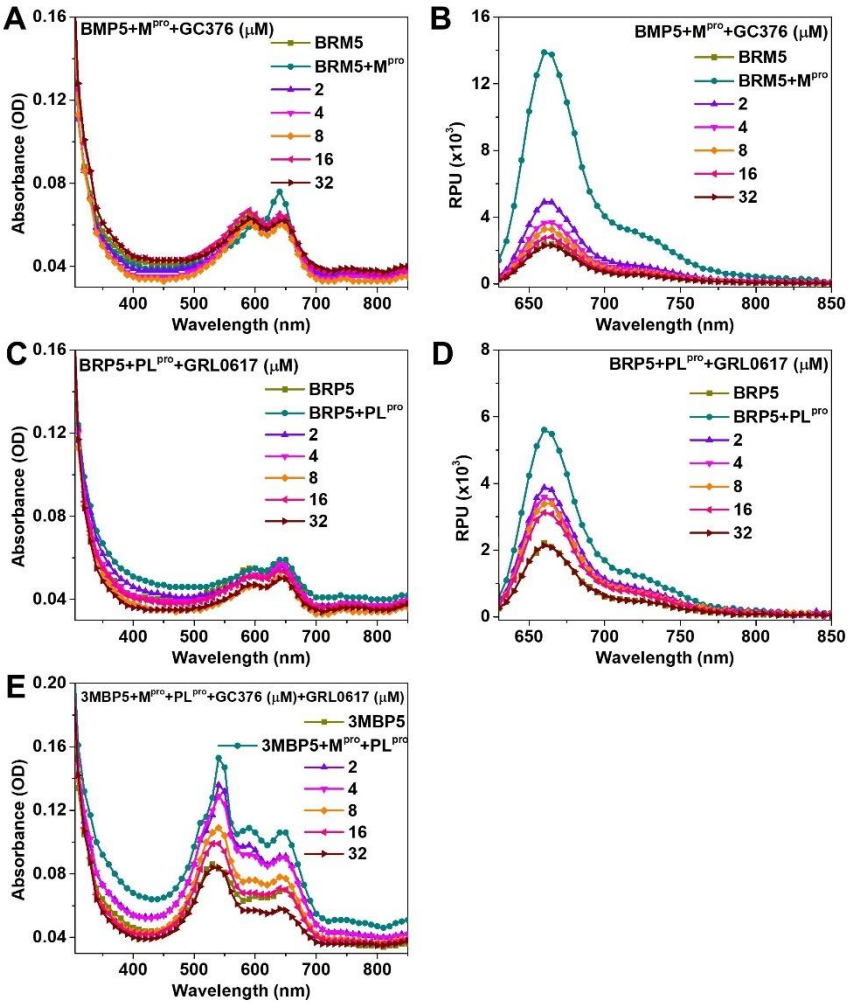

Figure S30. Each probe was incubated with the protease. Here, 2.0 μM of BRM5, BRP5, and 3MBP5 were incubated with 100 nM M^{pro} and 1000 nM PL^{pro} as well as different concentrations of GC376 and GRL0617. (A-B) UV−vis absorption and fluorescence spectra of BRM5 shows that GC376 inhibited the enzymatic activity of M^{pro}. (C-D) UV−vis absorption and fluorescence spectra of BRP5 shows that GRL0617 inhibited the enzymatic activity of PL^{pro}. (E) UV−vis absorption spectra of 3MBP5 shows that GC376 and GRL0617 inhibited the enzymatic activity of M^{pro} and PL^{pro}.

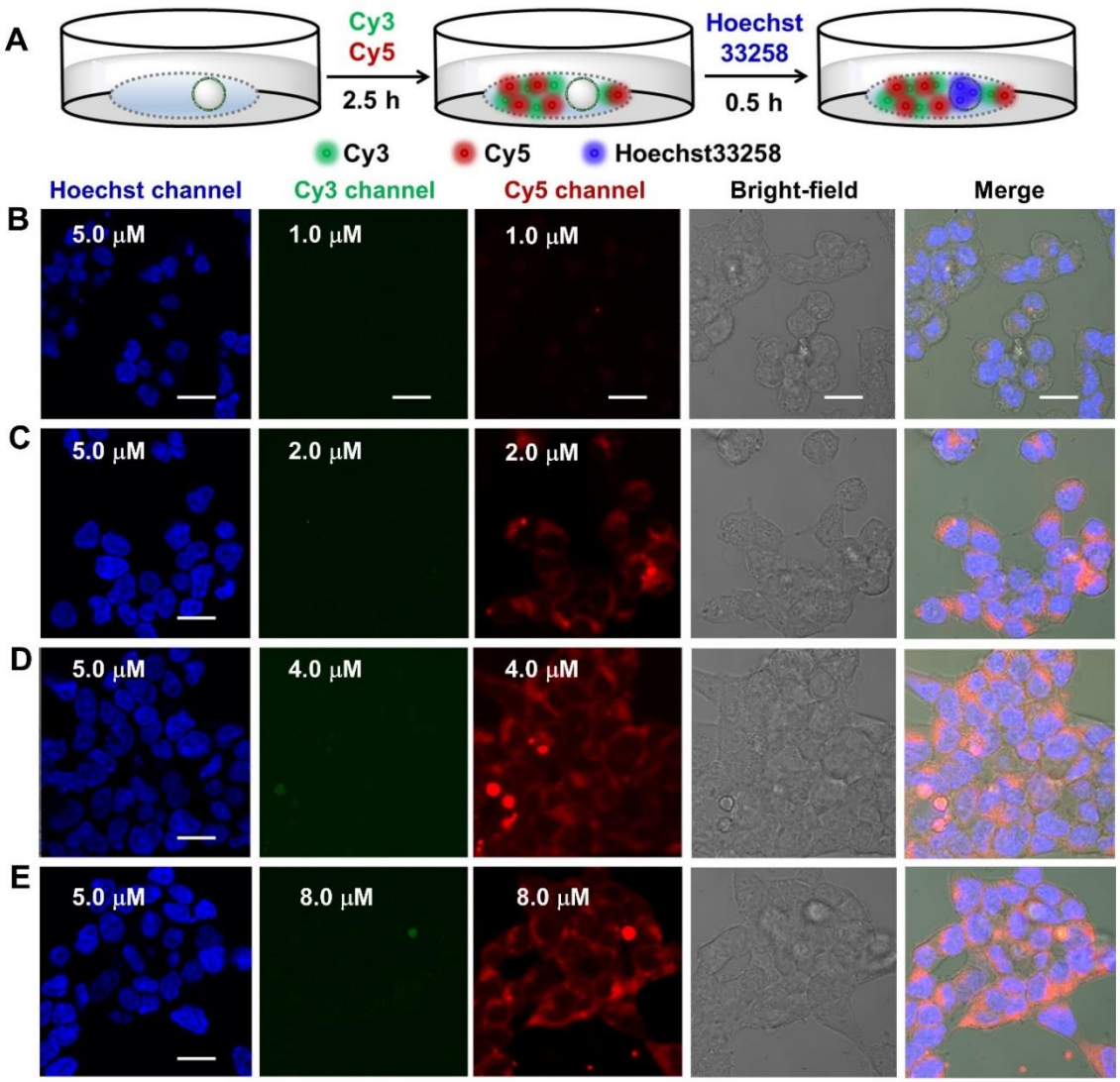

Figure S31. Confocal laser scanning microscopy (CLSM) images of HEK293T cells after incubation with different concentrations of Cy3 (1.0 μM, 2.0 μM, 4.0 μM and 8.0 μM) and Cy5 (1.0 μM, 2.0 μM, 4.0 μM and 8.0 μM) for 3 h, and 5.0 μM Hoechst 33258 for 30 min. The scale bar is 20 μm.

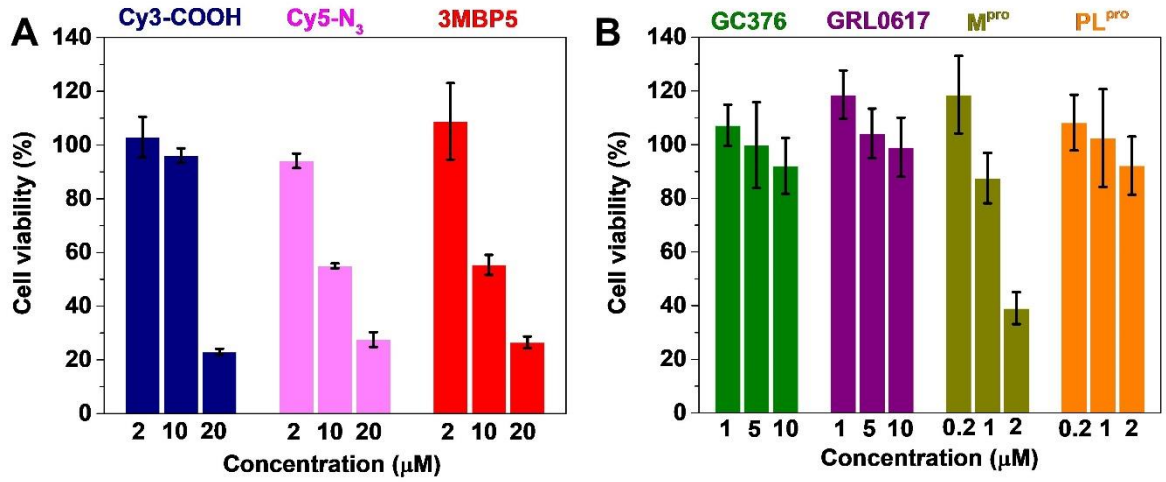

Figure S32. Metabolic activity of HEK 293T cells were studied with (A) (2.0 μM, 10.0 μM and 20.0 μM) Cy3-COOH, (2.0 μM, 10.0 μM, and 20.0 μM) Cy5-N_3, (2.0 μM, 10.0 μM, and 20.0 μM) 3MBP5; (B) (1.0 μM, 5.0 μM, and 10.0 μM) GC376, (1.0 μM, 5.0 μM, and 10.0 μM) GRL0617, (0.2 μM, 1.0 μM, and 2.0 μM) M^{pro}, and (0.2 μM, 1.0 μM, and 2.0 μM) PL^{pro} for 48 h using a fluorescence resazurin assay. The results show that 10 μM of Cy5-N_3 and 3MBP5, and 2 μM M^{pro} are obvious cytotoxic.

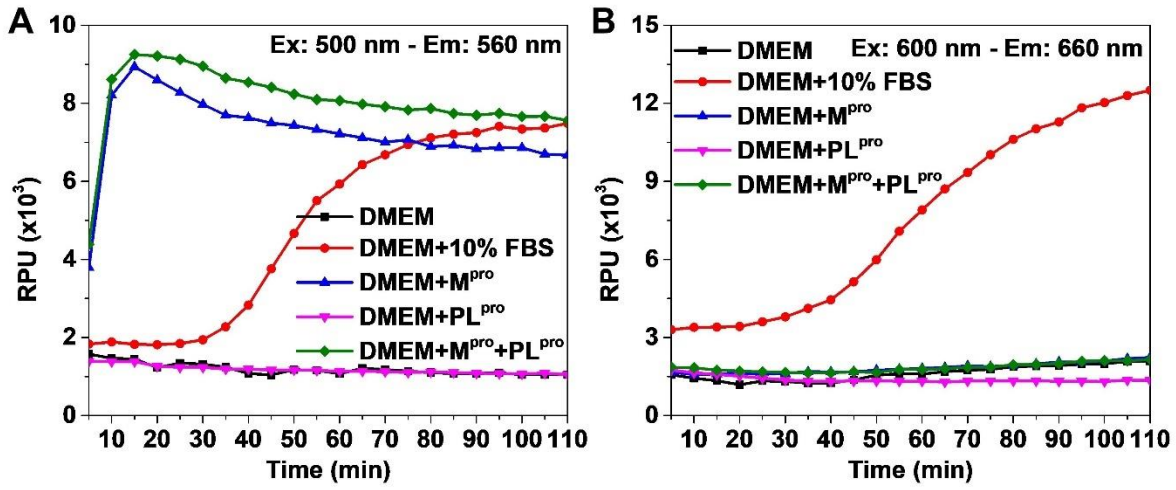

Figure S33. Time-dependent fluorescence spectra of 2.0 μM 3MBP5 after incubation with DMEM, DMEM with 10% FBS, DMEM with M^{pro}, DMEM with PL^{pro}, and DMEM with both M^{pro} and PL^{pro} for 110 mins under the excitation wavelength of (A) 500 nm or (B) 600 nm.

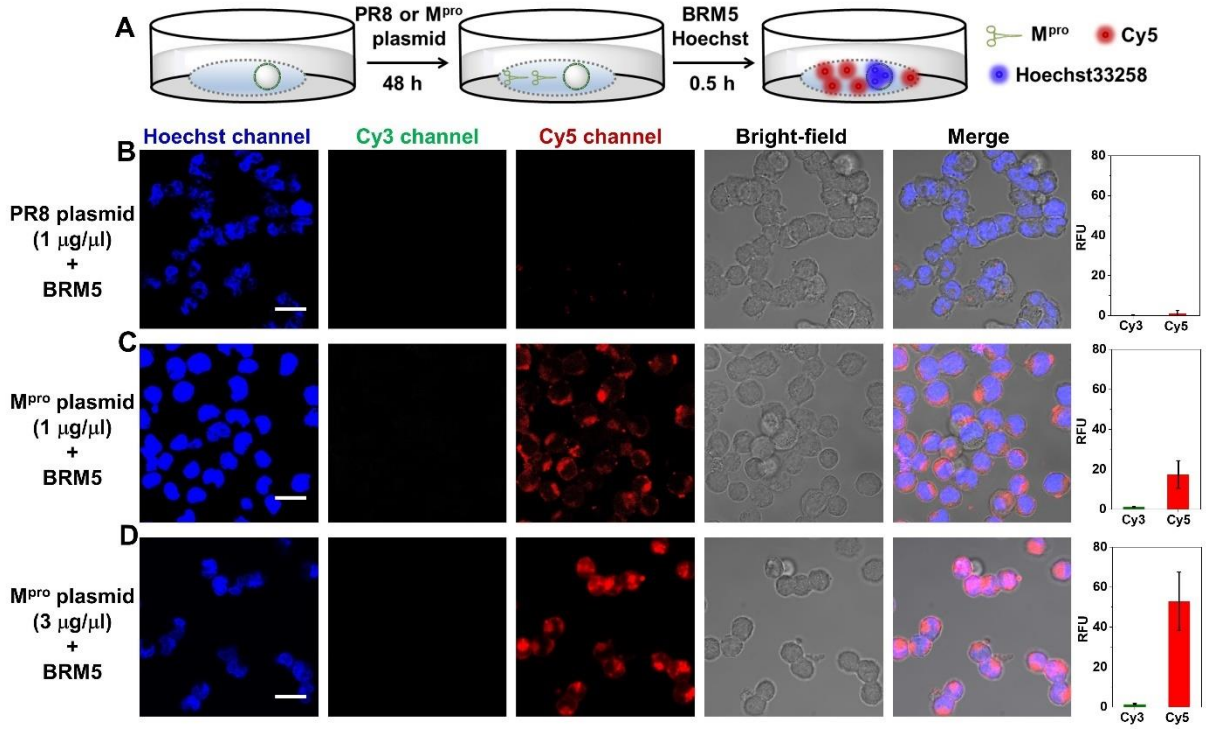

Figure S34. (A) Experimental scheme of HEK 293T cells after incubation with PR8 plasmid, M^{pro} plasmid and BRM5. The CLSM images and mean fluorescence intensity of HEK 293T cells after incubation with (B) 1.0 μg/μl PR8 plasmid, (C) 1.0 μg/μl M^{pro} plasmid, and 3.0 μg/μl M^{pro} plasmid for 48 h, 2.0 μM BRM5, and 5.0 μM Hoechst 33258 for 30 min. The scale bar is 20 μm.

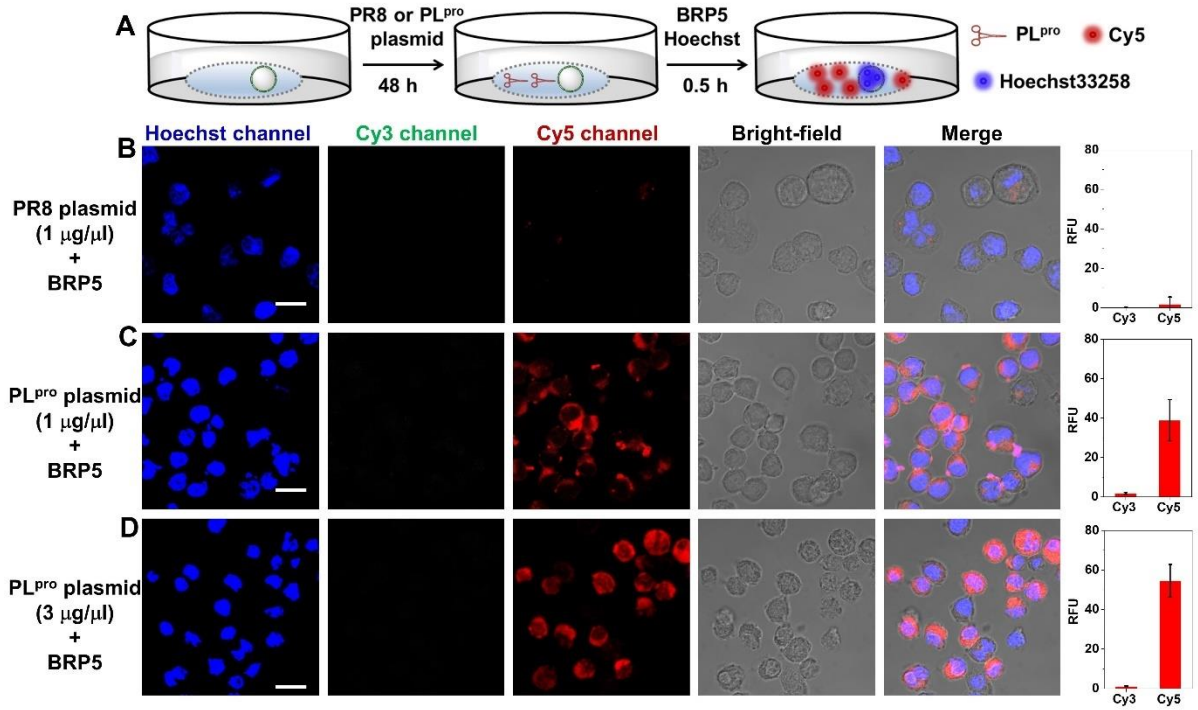

Figure S35. (A) Experimental scheme of HEK 293T cells after incubation with PR8 plasmid, PL^{pro} plasmid and BRP5. The CLSM images and mean fluorescence intensity of HEK 293T cells after incubation with (B) 1.0 μg/μl PR8 plasmid, (C) 1.0 μg/μl PL^{pro} plasmid, and (D) 3.0 μg/μl PL^{pro} plasmid for 48 h, 2.0 μM BRP5, and 5.0 μM Hoechst 33258 for 30 min. The scale bar is 20 μm.

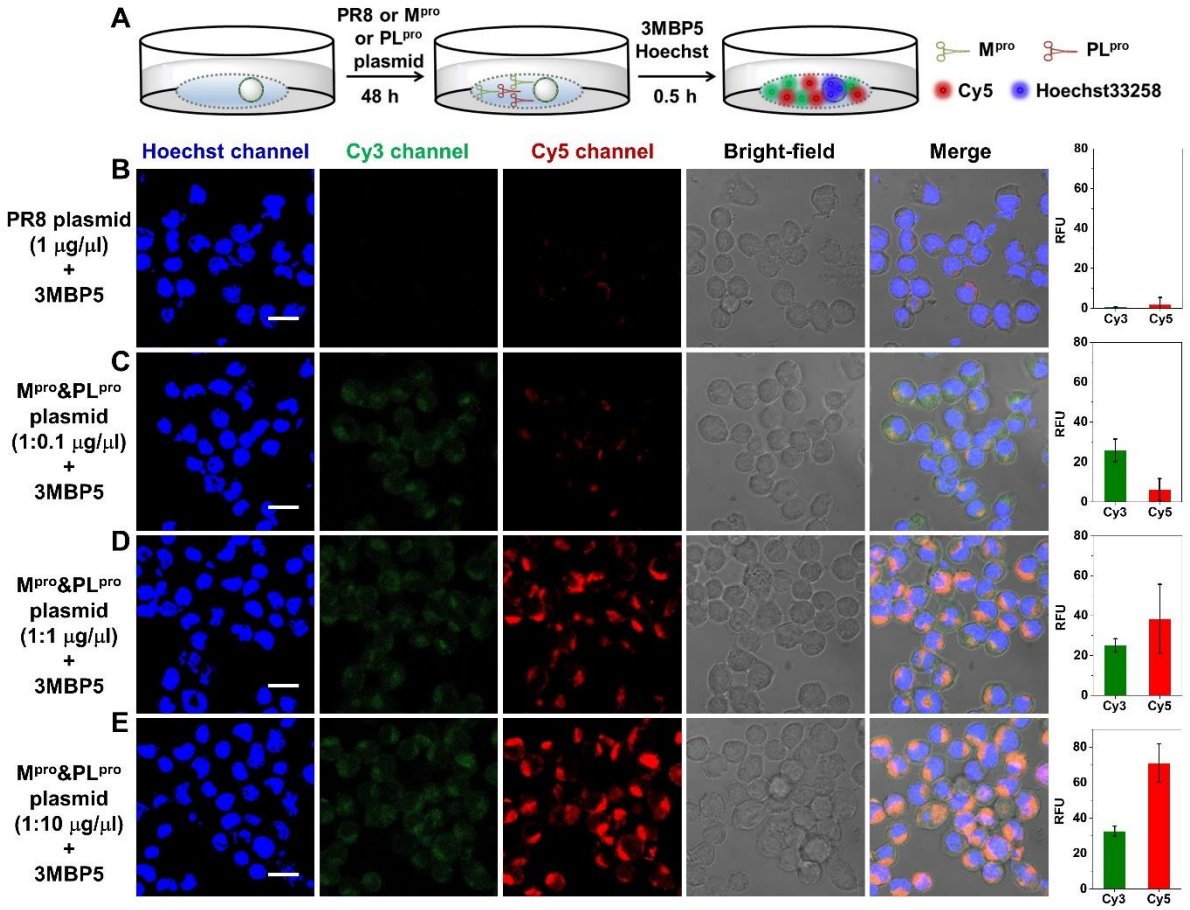

Figure S36. (A) Experimental scheme of HEK 293T cells after incubation with PR8 plasmid, M^{pro} plasmid and 3MBP5. The CLSM images and mean fluorescence intensity of HEK 293T cells after incubation with (B) 1.0 μg/μl PR8 plasmid, (C) 1.0 μg/μl M^{pro} and 0.1 μg/μl PL^{pro} plasmids, (D) 1.0 μg/μl M^{pro} and 1.0 μg/μl PL^{pro} plasmids, and (E) 1.0 μg/μl M^{pro} and 10.0 μg/μl PL^{pro} plasmids for 48 h, 2.0 μM BRM5, and 5.0 μM Hoechst 33258 for 30 min. The scale bar is 20 μm.

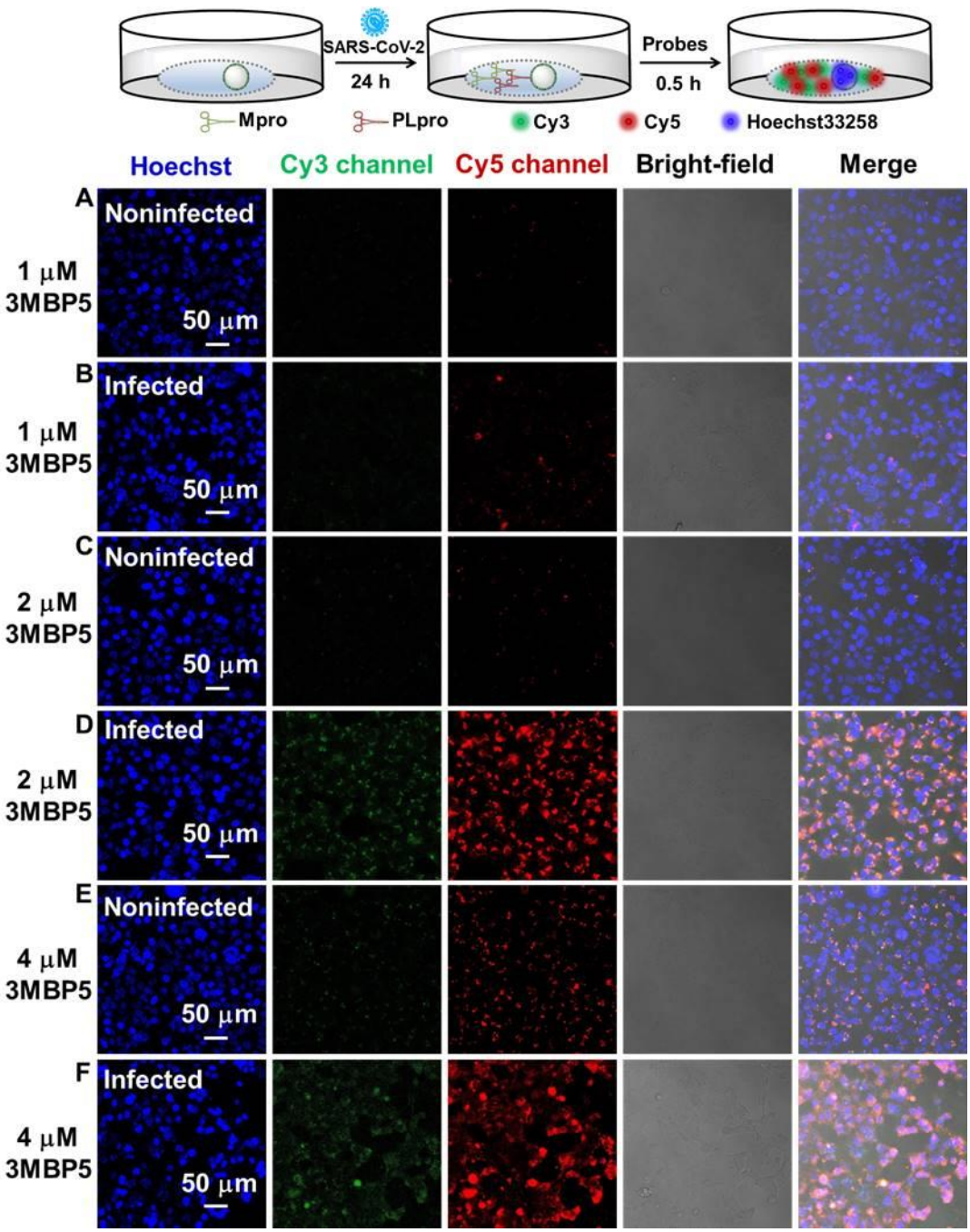

Figure S37. CLSM images of (A, C and E) SARS-CoV-2 noninfected or (B, D and F) infected TMPRSS2-Vero cells after incubation with different concentrations of (1.0 μM, 2.0 μM and 4.0 μM) 3MBP5 and 5.0 μM Hoechst 33258 for 30 min. The scale bar is 50 μm.

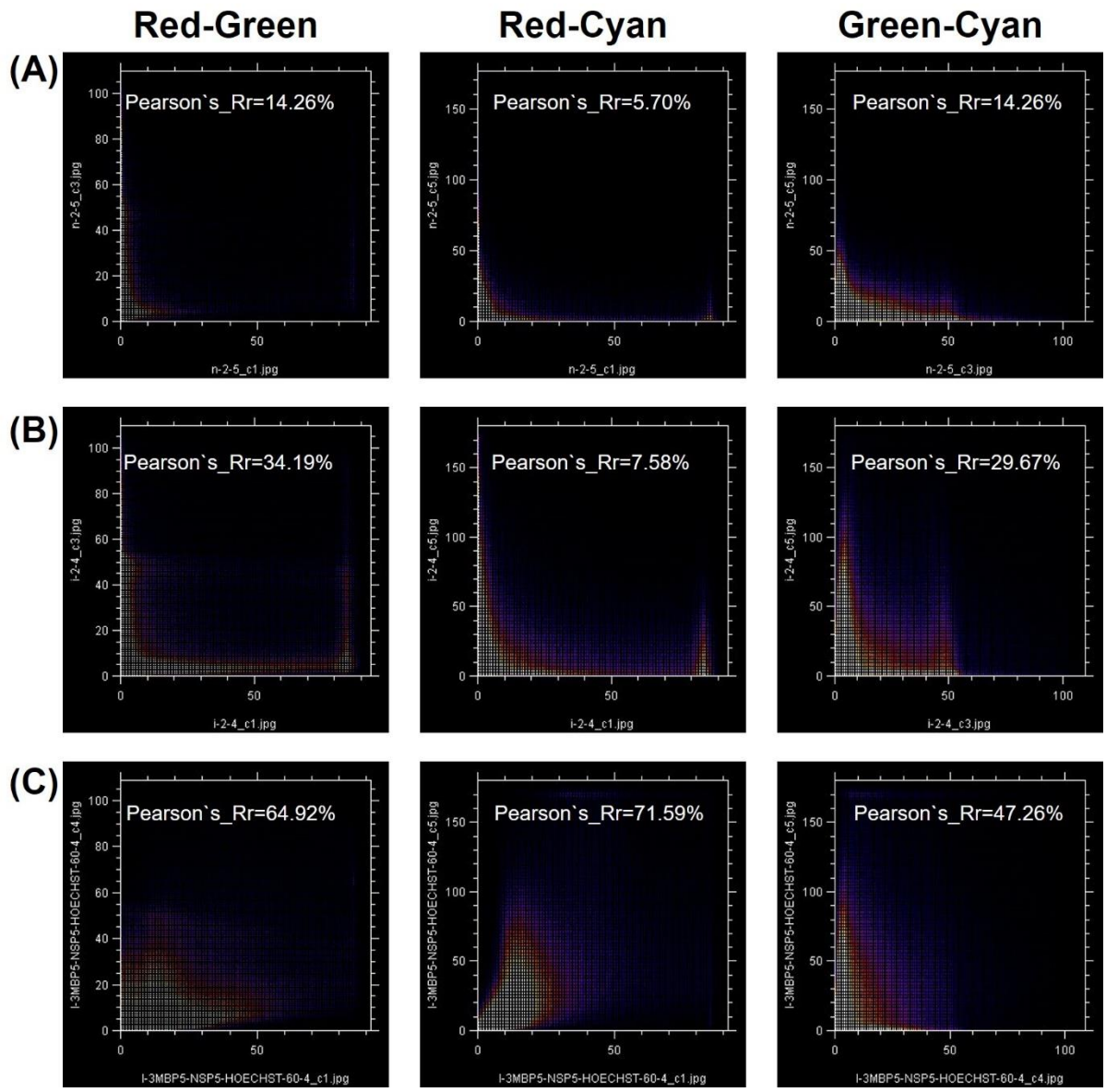

Figure S38. The Pearson correlation coefficient of co-localization between red, green and cyan fluorescence from (A) noninfected cells after incubation with 3MBP5 and Alexa488-labeled SARS-CoV-2 nucleocapsid, (B) infected cells after incubation with 3MBP5 and Alexa488-labeled SARS-CoV-2 nucleocapsid antibody, and (C) infected cells after incubation with 3MBP5 and Alexa488-labeled SARS-CoV-2 M^{pro} antibody.

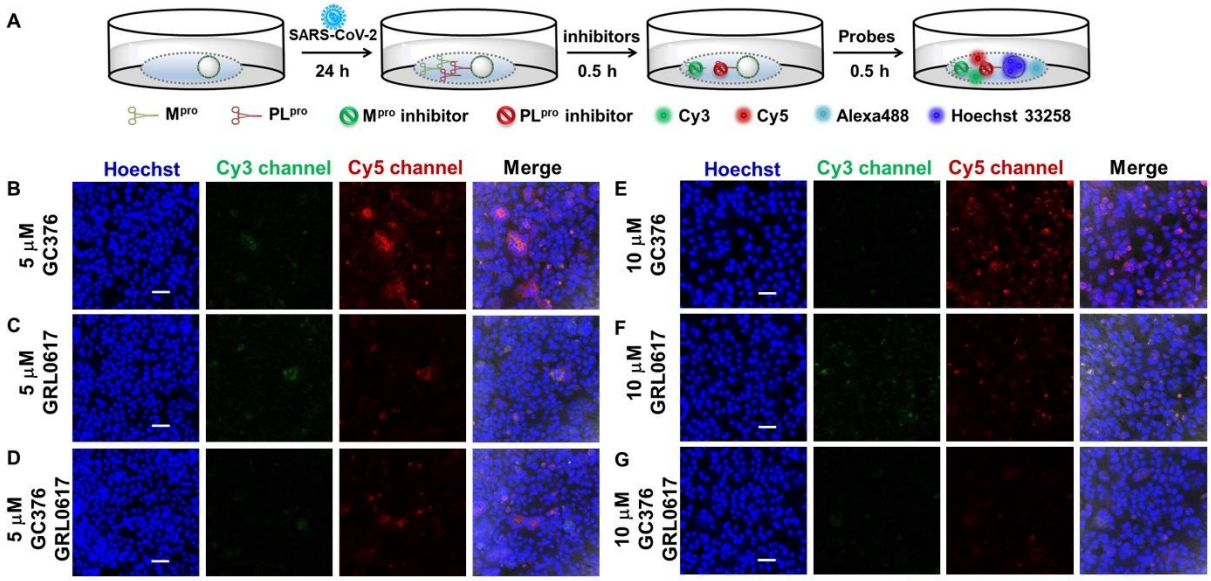

Figure S39. (A) Experimental scheme of SARS-CoV-2 infected TMPRSS2-Vero cells after incubation with different concentrations of M^{pro} inhibitor and PL^{pro} inhibitor for 1 h, 2.0 μM 3MBP5, and 5.0 μM Hoechst 33258 for 30 min. (B) 5 μM GC376; (C) 5 μM GRL0617; (D) 5 μM GC376 and GRL0617; (E) 10 μM GC376; (F) 10 μM GRL0617; (G) 10 μM GC376 and GRL0617. The scale bar is 50 μm.

References:

1. Froggatt, H.M., Heaton, B.E. & Heaton, N.S. Development of a Fluorescence-Based, High-Throughput SARS-CoV-2 3CLpro Reporter Assay. *Journal of Virology* **94**, e01265-01220 (2020).
2. Rut, W. *et al.* Activity profiling and crystal structures of inhibitor-bound SARS-CoV-2 papain-like protease: A framework for anti-COVID-19 drug design. *Sci Adv* **6** (2020).
3. Penalver, L. *et al.* A Ligand Selection Strategy Identifies Chemical Probes Targeting the Proteases of SARS-CoV-2. *Angew Chem Int Ed Engl* **60**, 6799-6806 (2021).
4. Cheng, Y. *et al.* Protease-Responsive Prodrug with Aggregation-Induced Emission Probe for Controlled Drug Delivery and Drug Release Tracking in Living Cells. *Anal Chem* **88**, 8913-8919 (2016).
5. Lyon, R.P. *et al.* Self-hydrolyzing maleimides improve the stability and pharmacological properties of antibody-drug conjugates. *Nat Biotechnol* **32**, 1059-1062 (2014).
6. Cheng, Y. *et al.* A Multifunctional Peptide-Conjugated AIEgen for Efficient and Sequential Targeted Gene Delivery into the Nucleus. *Angew Chem Int Ed Engl* **58**, 5049-5053 (2019).